Reviewed Preprint
v1 • August 6, 2025
Not revised

Reviewed Preprint
v2 • June 3, 2026
Revised by authors

For correspondence:
agnese.serafini@unipd.it

Competing interests: No competing interests declared

Funding: See page 34

Reviewing editor: Bavesh D Kana, University of the Witwatersrand, South Africa

Mycobacterium tuberculosis partitions the Krebs cycle under iron starvation

Agnese Serafini[a], Acely Garza-Garcia[b], Davide Sorze[a], Luiz Pedro Sorio de Carvalho[b,c], Riccardo Manganelli[a]

[a]Department of Molecular Medicine, University of Padova, Padova, Italy • [b]Mycobacterial Metabolism and Antibiotic Research Laboratory, The Francis Crick Institute, London, United Kingdom • [c]Chemistry Department, The Herbert Wertheim UF Scripps Institute for Biomedical Innovation & Technology, Jupiter, United States

eLife Assessment

This well-designed, **valuable** study uses isotope tracing to analyse how iron limitation alters TCA cycle metabolism in Mycobacterium tuberculosis, revealing potential antibiotic targets for non-replicating bacteria in the host. The evidence is **solid**, providing insights into metabolic remodelling under iron-limited conditions.

https://doi.org/10.7554/eLife.107596.2.sa3

Abstract

In this study, we investigated how iron limitation alters central metabolism in *Mycobacterium tuberculosis* using metabolomics and stable isotope tracing. Our findings reveal a well-orchestrated metabolic program to enable Krebs cycle activity despite the inefficient action of its iron-dependent enzymes. Under such conditions, carbon flux through the oxidative branch of the Krebs cycle is stalled, resulting in the accumulation of metabolites that are partially secreted. As a result, carbon flux from glycolysis is partially diverted to the reductive branch of the Krebs cycle to support the production of oxaloacetate and malate through the activity of phosphoenolpyruvate carboxykinase and pyruvate carboxylase. Both branches terminate with the synthesis of malate, which is secreted. This unprecedented split of the Krebs cycle and malate secretion in a bacterial pathogen facilitates the continuous flow of carbon through the core of carbon metabolism, overcoming the metabolic stalling triggered by iron starvation.

Introduction

Over the past decade, mounting evidence has indicated a clear correlation between central metabolism and antibiotic resistance. It has been demonstrated that clinically relevant mutations in genes encoding core metabolic enzymes are associated to antibiotic resistance (Lopatkin et al. 2021) and tolerance (Hicks et al. 2018). Furthermore, secondary or "collateral" effects of antibiotic action involve alterations to central carbon metabolism (CCM) (Wang et al. 2019; Kawai et al. 2019) and specific metabolic states affect their efficacy (Allison et al. 2011; Lim et al. 2021; Lopatkin et al. 2019; Schrader et al. 2021).

Mycobacterium tuberculosis (*Mtb*), the causative agent of tuberculosis (TB), has been recently included in the Bacterial Priority Pathogen List of the World Health Organization (WHO, 2024) due to its intrinsic resistance to antibiotics and the increased spreading of multi-drug-resistant strains. Since the 1960s, only three new drugs have been approved for the treatment of TB (Murray et al. 2015; Zheng & Av-Gay 2016; Dartois & Dick 2024), and resistance to these new antibiotics is increasing. It is therefore critical that new medicines are developed to treat this infection. For more efficient antibiotic discovery, we must gain a more comprehensive understanding of the physiology and metabolism of *Mtb*. This knowledge will help identify novel vulnerabilities and inform the design of more effective therapeutic strategies.

During infection pathogenic bacteria are subject to nutritional immunity, a process in which the host alters metal availability to intoxicate or starve the invading pathogens (Murdoch & Skaar 2022). Metals are essential micronutrients that play structural, signalling or catalytic roles in most of cellular processes. Many enzymes of central metabolism depend on metals for their activity, however the effects of nutritional immunity on CCM have not been extensively investigated (Serafini 2021). Experimental evidence indicates that *Mtb* is exposed to iron starvation during infection (Kurthkoti et al. 2017; Wells et al. 2013; Fang et al. 2015; Madigan et al. 2015; Pisu et al. 2020). This study aims to examine the relationship between iron homeostasis and CCM, a complex and understudied aspect of *Mtb* metabolism. *Mtb* exposed to prolonged and severe iron starvation exhibits a reduction in growth rate until replication is arrested, yet, cells remain viable (Kurthkoti et al. 2017). Based on the publicly available transcriptomic and proteomic data of H37Rv *Mtb* strain grown under iron limitation (Dataset S1 and Kurthkoti et al. 2017; Wong et al. 1999; Serafini et al. 2013), we have recently proposed a model that explains how this pathogen might adapt its core of CCM to limited iron availability (Serafini 2021). We proposed that *Mtb*: i) reduces the activity of the Krebs cycle due to the compromised activity of its iron-dependent enzymes, which consequently reduces the production of $FADH_2$, NADH and ATP; ii) activates an iron-independent pathway, the glyoxylate shunt, to maintain succinate and malate production; iii) secretes succinate to maintain an energised cell membrane, bypassing the reduced ATP synthase activity.

The aim of the present study is to test these predictions thereby clarifying the effect of iron starvation on *Mtb* metabolism. We monitored metabolite levels using liquid chromatography coupled to mass spectrometry and employed ^{13}C isotope tracing to identify the metabolic pathways active under iron starvation. These experiments were conducted under the same growth conditions used in the more comprehensive transcriptomic study (Kurthkoti et al. 2017), which, like the other published studies on iron limitation (Wong et al. 1999; Serafini et al. 2013), included two carbon sources in the growth medium, glucose and glycerol. To circumvent genomic background-dependent effects, the work was performed in two *Mtb* strains with different metabolic capacities, H37Rv and Erdman (Serafini et al. 2019; Marrero et al. 2010).

Results

Severe growth defects accompany iron limitation

As demonstrated previously (Kurthkoti et al. 2017), *Mtb* exposed to severe iron starvation enters a non-replicative state that can persist for months. This severe iron starvation was achieved by subculturing bacteria in the absence of a source of Fe^{3+}, followed by the addition of the Fe^{3+} chelator deferoxamine (DFO), to trap any residual ion. Equivalent conditions were used in our laboratory to reproduce the growth arrest phenotype in Erdman and H37Rv (Figure 1A-D). As expected, the absence of a Fe^{3+} source (0 µM $FeCl_3$) resulted in a growth slowdown, while the addition of DFO (0 µM $FeCl_3$ + DFO) led to growth arrest (Figure 1A and B). In the latter, Erdman exhibited an apparent decline in viability over several weeks (Figure 1D) compared to H37Rv (Figure 1C). This decline could be attributed to a loss of viability, or more pronounced clumping of the cells in Erdman cultures (data not shown), that resulted in a reduction in the number of colony-forming units (CFUs), or to the cells entering an unculturable state (Kurthkoti et al. 2017).

Previous studies have shown that replication-arrest-inducing stress conditions such as hypoxia and nutrient starvation (Eoh & Rhee 2013; Rao et al. 2008; Gengenbacher et al. 2010) reduce ATP production and alter the $NADH/NAD^+$ ratio. Transcriptomics data shows that upon Fe^{3+} depletion, *Mtb* down-regulates the operon encoding ATP synthase and the type I NADH dehydrogenase (Dataset S1 and Kurthkoti et al. 2017; Serafini et al. 2013). We examined the levels of ATP and the $NADH/NAD^+$ ratio in H37Rv and Erdman strain. Surprisingly, ATP levels (Figure 1G and H, Figure 1–figure supplement 1A and B) did not decrease upon Fe^{3+} depletion and showed a trend very similar to the condition with sufficient Fe^{3+}. In contrast, we did see a significant increase in the $NADH/NAD^+$ ratio upon Fe^{3+} depletion compared to the presence of sufficient Fe^{3+} (Figure 1I, Figure 1–figure supplement 1C and D), indicating an

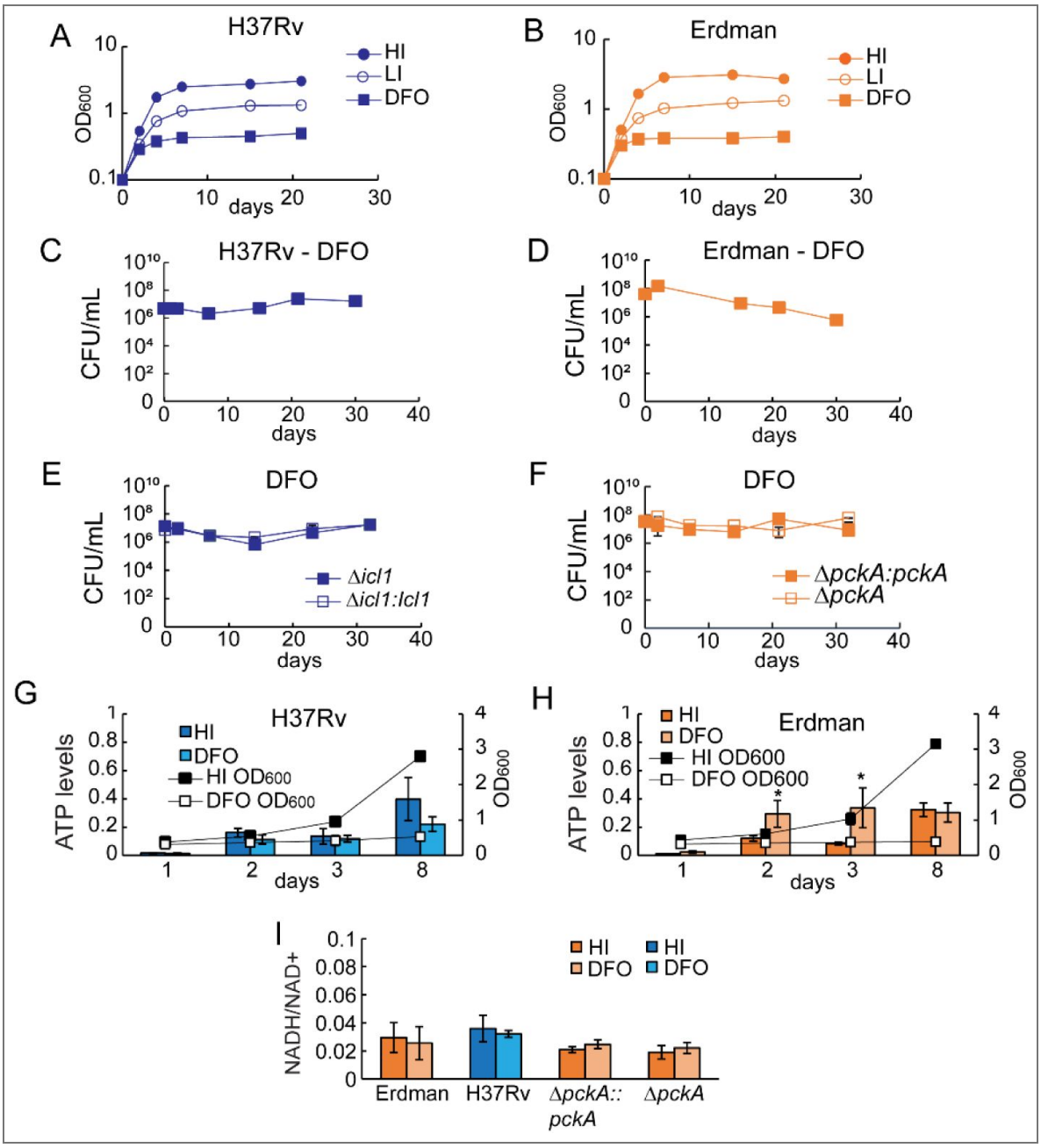

Figure 1. Survival to Fe^{3+} starvation in *Mtb* H37Rv and Erdman strains.

Cells were exposed to 50 μM $FeCl_3$ (HI: High Iron), 0 μM $FeCl_3$ (LI: Low Iron,) or 0 μM $FeCl_3$+ DFO (DFO). Growth was monitored for 3 weeks by measuring OD_{600} (A, B), and survival was monitored for more than 4 weeks by CFU/mL (C, D, E, F). The charts show one experiment representative of 2-3 independent experiments. The CFU/mL charts show average and average deviation of two technical replicates of one independent experiment. G, H) ATP levels and growth (OD_{600}) after 1, 2, 3 and 8 days in DFO. ATP levels were calculated as μM of ATP molecules in about 10^7 cells (0.1 optical density at 600 nm). The data are the average and standard deviation of three independent experiments and three technical replicates each. I) NADH/NAD+ ratio detected after 3 days of exposure to DFO. The data are the average and standard deviation of two independent experiments and two technical replicates. The p-values were calculated against the HI condition. * = p value < 0.05.

accumulation of NADH. The concordant results between the two wild type stains, supports the hypothesis that the loss of viability in Erdman is not due to cell death, and indicates that in *Mtb* Fe^{3+} starvation causes a metabolic and physiological stress that is distinct from that observed in hypoxia and nutrient starvation (Rao et al. 2008; Gengenbacher et al. 2010; Eoh & Rhee 2013).

Slowdown of the Krebs cycle activity

Most genes encoding enzymes involved in the Krebs cycle exhibit a reduction in their expression levels over a two-week period in Fe^{3+}-starved H37Rv (Dataset 1 and Kurthkoti et al. 2017). This finding indicates that the activity of this pathway may be reduced in such a condition. The levels of Krebs cycle intermediates were examined following an eight-day exposure to Fe^{3+}-replete conditions (50 μM $FeCl_3$, termed HI henceforth) and Fe^{3+}-limiting conditions (0 μM $FeCl_3$ and 0 μM $FeCl_3$+DFO, termed LI and DFO, respectively, henceforth). As the metabolomics analysis demonstrated highly comparable outcomes in the LI and DFO conditions, the subsequent sections will focus on the comparison between HI and DFO. Please refer to supplementary data (Supplement file section I) for a detailed analysis in the LI condition.

In H37Rv, a consistent increase, exceeding a 100-fold change (FC), in the intracellular levels of pyruvate and α-ketoglutarate was observed in DFO compared to HI (Figure 2A). The accumulation of these two metabolites is in line with the downregulation of the *aceE*, *dlaT* and *lpdC* genes (Dataset S1 and Kurthkoti et al. 2017), which encode subunits of the pyruvate dehydrogenase (PDH) and the α-ketoglutarate dehydrogenase (KDH) complexes (Tian et al. 2005; Shi & Ehrt 2006; Maksymiuk et al. 2015). This accumulation is consistent with the existence of two stalling points at which the activity of the Krebs cycle is impeded, one before the cycle (PDH) and one at the KDH level. It is likely that the blockage at the level of pyruvate results in a slowdown the flux through glycolysis. The downregulation of glycolytic genes (Dataset 1 and Kurthkoti et al. 2017) lends support to this hypothesis. A smaller increase in the levels of (iso)citrate was observed, with a 2- to 4-FC in two independent experiments (Figure 2A). This increase may be attributed to two potential mechanisms: i) citrate accumulation resulting from the reduced activity of the iron-dependent aconitase (Acn), which is also known to be down-regulated (Kurthkoti et al. 2017; Wong et al. 1999; Serafini et al. 2013); ii) isocitrate accumulation due to blockage of the Krebs cycle at the KDH level. The major fold increase (~100-fold) in αKG compared to (iso)citrate is consistent with the irreversibility of the isocitrate dehydrogenase reaction, which drives carbon flux from isocitrate toward αKG but not in the reverse direction. As a result, isocitrate cannot accumulate to the same extent. Further, the intracellular threshold of these two metabolites may differ leading the cells to divert (iso)citrate into other metabolic pathways, limiting its accumulation.

The succinate pool exhibited a statistically significant decrease in DFO, with intensity varying from 0.3- to 0.8-FC in two independent experiments (Figure 2A). No relevant alterations were observed in the levels of fumarate and malate. These results seem to contrast with the observation that genes encoding enzymes involved in the synthesis of fumarate and malate (fumarate reductase/Frd, fumarase/Fum and succinate dehydrogenase/Sdh) are iron-dependent and downregulated under Fe^{3+} starvation (Dataset S1 and Kurthkoti et al. 2017) and therefore their activity should be lower in such conditions. Surprisingly, the genes encoding the α-ketoglutarate ferredoxin-oxidoreductase KorAB complex (Baughn et al. 2009) are induced (Kurthkoti et al. 2017) suggesting that despite its iron-dependent nature, its activity is necessary to produce succinyl-CoA and then succinate from α-ketoglutarate.

As observed in H37Rv, in the Erdman strain (Figure 2–figure supplement 1A) there is a substantial intracellular accumulation of pyruvate and α-ketoglutarate (>10 FC) and a more modest accumulation of (iso)citrate (1.2-2.8 FC, in four independent experiments) in DFO. No major changes were observed in the levels of malate, fumarate and succinate.

In conclusion, when experiencing Fe^{3+} starvation, *Mtb* slows down the activity of the Krebs cycle, and pyruvate conversion to acetyl-CoA and α-ketoglutarate conversion into succinyl-CoA may represent two distinct checkpoints in this process.

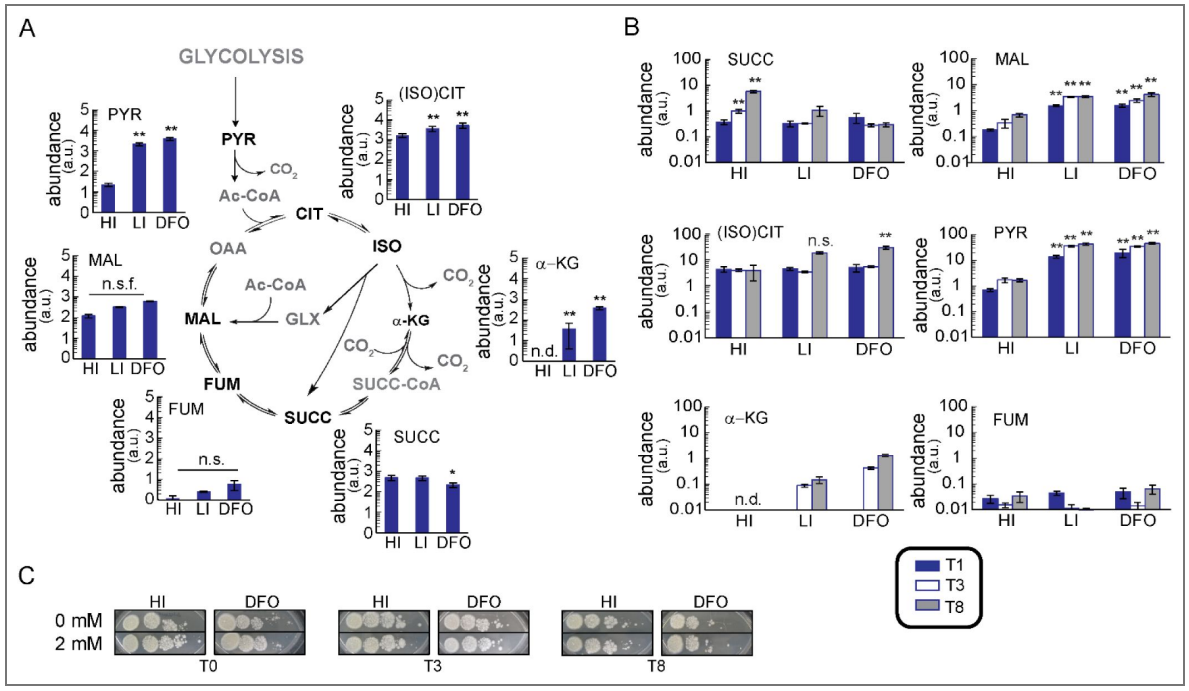

Figure 2. Intracellular and extracellular levels of metabolites in H37Rv.

Cells were exposed to 50 μM $FeCl_3$ (HI: High Iron), 0 μM $FeCl_3$ (LI: Low Iron,) or 0 μM $FeCl_3$+ DFO (DFO). The analysed metabolites are shown in black in the schematic pathways. A) Intracellular polar metabolites levels at 8 days; the y-axis is shown on Log_{10} scale tick labels (0–5) represent the exponents of 10 (10^0–10^5); values are reported in arbitrary units. B) Extracellular polar metabolites levels at 1, 3 and 8 days. The plots show the normalised levels of metabolites. The data represent the average and the standard deviation of four biological replicates from an independent experiment, representative of two independent experiments. The y-axis is shown on is in Log_{10} scale, values are reported in arbitrary units. C) Viability of H37Rv from one independent experiment. Cells were grown in liquid medium in HI and DFO conditions and in the presence of 2 mM of succinate. Aliquots of cells were collected after 0, 3 and 8 days and diluted to same final OD_{600}; 5 μL of 10-fold serial dilutions were plated on 7H10. Growth was recorded after 19-25 days. The p-values were calculated against the HI condition and independently for the two experiments, the highest p-value was reported. n.s.f.= non-significant fold change, the observed trend change was different between independent experiments; n.s.= non-significant, p value >0.05; n.d.= non-detected; * =p value <0.05; ** =p value <0.01. Ac-CoA: acetyl-CoA; CIT: citrate; FUM: fumarate; α-KG: α-ketoglutarate; ISO: isocitrate; (ISO)CIT: isocitrate and citrate; MAL: malate; OAA: oxaloacetate; PYR: pyruvate; SUCC: succinate; SUCC-CoA: succinyl-CoA.

Substantial secretion of metabolic intermediates

The secretion of succinate has been linked to the maintenance of membrane potential in hypoxic growth-arrested *Mtb* (Eoh & Khee 2013). It has been demonstrated that in such condition the extracellular succinate levels increase and that the inhibition of its secretion (by supplementing the medium with succinate) causes alteration of the proton motive force and cell death (Eoh & Khee 2013). We hypothesised that succinate could have a similar role in DFO-treated cells (Serafini 2021). Levels of extracellular succinate were therefore monitored over a week period (1, 3 and 8 days). Unexpectedly, no change in succinate levels was observed in DFO, rather, a significant increase was noted in HI (Figure 2B and Figure 2–figure supplement 1B). Furthermore, the succinate levels were lower in DFO compared to the HI condition. Since *Mtb* cells remain viable in DFO (Figure 1C and D), it can be concluded that the secretion of succinate is not a crucial factor in maintaining cell survival and membrane potential in such condition. This conclusion was confirmed by the observation that DFO-treated cells exposed to 2 mM succinate in the order to inhibit its secretion (Eoh & Khee 2013), remained viable (Figure 2C and Figure 2-figure supplement 1C), in contrast to the results observed during hypoxia.

Surprisingly, higher levels of several Krebs cycle intermediates were found in the culture filtrate of DFO compared to HI cultures, with minor discrepancies between the H37Rv (Figure 2B) and Erdman (Figure 2–figure supplement 1B) strain. α-ketoglutarate, (iso)citrate, malate and pyruvate are secreted in substantial quantities and their levels increase over time, with the exception of fumarate and succinate. The levels of pyruvate and α-ketoglutarate increase by more than 10-fold, while those of (iso)citrate rise by 2- to 10-fold under Fe^{3+} starvation. The high levels of extracellular pyruvate, α-ketoglutarate and (iso)citrate are consistent with the elevated intracellular levels. It is noteworthy that malate levels exhibit a substantial increase, approximately 10-fold, in DFO compared to HI conditions despite similar intracellular levels under the two conditions. This increase occurs after one day of DFO exposure in H37Rv (Figure 2B) and at a later stage in the Erdman strain (Figure 2-figure supplement 1B). The analysis of ^{13}C incorporation in extracellular metabolites is consistent with the altered flow of carbon through the Krebs cycle (Figure 2-figure supplement 2A-H and Supplement file S*ection II*).

The decrease in CFU/mL in Erdman (Figure 1D) raised the possibility of cell lysis, that could explain the increase of extracellular malate despite of unchanged intracellular levels in DFO compared to HI conditions. If increased lysis had occurred, we would expect an overall increase in extracellular metabolites. However, extracellular fumarate and succinate levels did not increase in DFO both in Erdman strain and H37Rv (Figure 2B and Figure 2-figure supplement 1B). We also examined the levels of extracellular glutamate, an amino acid which abundance increase over a week in HI. As for fumarate, extracellular glutamate levels remained unchanged or decreased in DFO (Figure 2-figure supplement 2I and L) in Erdman and H37Rv. Therefore, we conclude that the observed increase of abundance of specific metabolites is not due to cell lysis.

As the intracellular malate pool is constant under HI and DFO conditions, this increase in malate secretion suggested that this metabolite may be utilised for the maintenance of membrane potential. The viability of DFO-treated cells in the presence of malate was evaluated (Figure 2-figure supplements 1C and 3A) but no effect was observed on survival. The substantial secretion of several metabolites prompted the hypothesis that they may collectively contribute to the maintenance of the membrane potential. The experiment was then repeated adding pyruvate, α-ketoglutarate, succinate, malate and fumarate individually (Figure 2-figure supplements 1C and 3A) and in combination, yet again we saw no loss of viability. These results suggest that the secretion of these metabolites under Fe^{3+} starvation is unrelated to the maintenance of the membrane potential.

Partitioning of carbon flux into oxidative and reductive branches of Krebs cycle

The transcriptomic data from Fe^{3+}-starved H37Rv (Kurthkoti et al. 2017; Serafini et al. 2013), shows upregulation of isocitrate lyase 1 (*icl1/Rv04671*) (Höner Zu Bentrup et al. 1999) and phosphoenolpyruvate carboxykinase A (*pckA*/*Rv0211*) (Marrero et al. 2010; Machova et al. 2015) genes (Dataset S1). To verify the effective operation of these metabolic routes, cells were fed with $^{13}C_3$-glycerol and the isotopic labelling profiles of multiple metabolites reporting on CCM were analysed (Figures 3 and 4).

Malate only partially derives from succinate oxidation

DFO-treated H37Rv shows a 50% reduction in labelled succinate compared to HI condition (Figure 3). This decrease is not observed in isocitrate and α-ketoglutarate, precursors of succinate. These discrepancies suggest that a slower rate conversion of α-ketoglutarate into succinyl-CoA and subsequently into succinate, and of isocitrate to succinate may occur in DFO. The down-regulation of KDH complex genes (Dataset S1 and Kurthkoti et al. 2017) supports the hypothesis related to α-ketoglutarate, however the up-regulation of *icl1* and *korAB* (see above) contradicts both hypotheses. The percentage of labelling observed in the malate pool (Figure 3) remains constant between the DFO and HI conditions. Notably, the percentage of malate labelling is significantly higher than that of succinate in DFO, indicating that some of the malate may not originate from succinate via fumarate. Unfortunately, the fumarate levels (Figure 3) were insufficient to permit the detection of labelling for this metabolite and verify if it is similar to malate rather than succinate. However, the comparison of the isotopologue distributions of malate and succinate confirms that some of the malate is not a product of succinate oxidation (Figure 3). Indeed, whereas in HI conditions the malate and succinate labelled pools show similar levels of M+1 and M+2 isotopologues (omitted isotopologue word after 'M+*n*' henceforth) and lower levels of M+3, in DFO M+2 succinate is more abundant compared to the M+1 and M+3, and M+3 malate is the most abundant (70 - 90% of total labelling) over M+1 and M+2 (Figure 3).

The DFO-treated Erdman strain does not show a marked decrease in the total labelling of succinate pool (Figure 4), and the isotopologue distribution shows that M+1 and M+2 are present at similar levels in the DFO and HI conditions. Similarly to H37Rv, in Erdman strain the malate labelled pool size was similar in DFO and HI conditions, and contains more M+3 in DFO compared to HI (40 – 50% of total labelling), with a clear decrease in M+1 an M+2 (Figure 4). In the Erdman strain, higher levels of fumarate were detected and ^{13}C incorporation could be evaluated. Surprisingly, the labelled fumarate pool contained only M+1 in all conditions (Figure 4), impeding a more precise tracking of its origin. This specific labelling profile of fumarate is likely linked to the specific medium used in the current work (Supplement file section III).

Altogether, these results strongly suggest that up to 50% of the malate pool is not derived from succinate oxidation under the DFO condition in *Mtb*.

Malate mainly derives from oxaloacetate reduction

The upregulation of *icl1* and *pckA* genes under Fe^{3+} condition (Kurthkoti et al. 2017; Serafini et al. 2013) suggests that malate may be produced via isocitrate lyase (ICL) and phosphoenolpyruvate carboxykinase (PCK) activities, despite the conflicting differences in the total labelling (Figure 3) between isocitrate and succinate (see above). The increase of these enzymatic activities was confirmed in the cell-free extracts (Figure 5A and B, Figure 5-figure supplement 1).

Figures 3 and 4-figure supplements 1 and 2 show 31 possible metabolic scenarios for the production of core of CCM intermediates when the glyoxylate cycle and/or the PCK anaplerotic route are active. These scenarios combine labelled and unlabelled pyruvate, phosphoenolpyruvate (PEP), acetyl-CoA and carbon dioxide molecules. Although they do not consider the re-circulation of metabolites in the global metabolic circuit, these series of reactions offer a useful perspective on identifying operating pathways. We compared these theoretical possibilities with our labelling

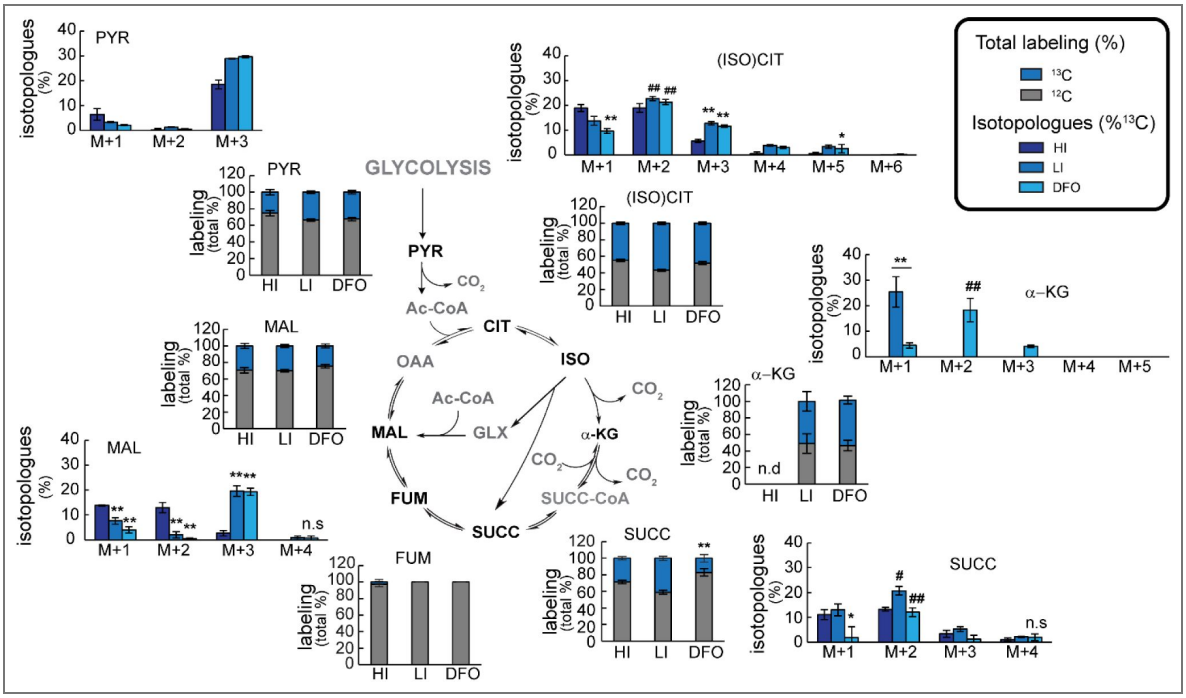

Figure 3. Percentage of labelled (^{13}C) and unlabelled (^{12}C) metabolites in H37Rv.

Metabolites were extracted from cells fed with $^{13}C_3$-glycerol for 8 days in 50 µM $FeCl_3$ (HI: High Iron), 0 µM $FeCl_3$ (LI: Low Iron) or 0 µM $FeCl_3$+ DFO (DFO). The analysed metabolites are shown in black in the schematic pathways. For each metabolite, but fumarate, two plots are shown. The stacked column plot shows the total percentage of labelled and unlabelled molecules per each metabolite pool; the clustered column plot shows the abundance in percentage of each isotopologue. The data represent the average and the standard deviation of four biological replicates from an independent experiment, representative of two independent experiments. The p-values were calculated independently for the two experiments and the highest p-value was reported. DFO/LI vs HI condition: * = p value<0.05; ** = p value <0.01; n.s.= non-significant. n.d.= non-detected. M2 vs M1: # = p value<0.05; ## = p value<0.01. Ac-CoA: acetyl-CoA; CIT: citrate; FUM: fumarate; α-KG: α-ketoglutarate; ISO: isocitrate; (ISO)CIT: isocitrate and citrate; MAL: malate; OAA: oxaloacetate; PYR: pyruvate; SUCC: succinate; SUCC-CoA: succinyl-CoA.

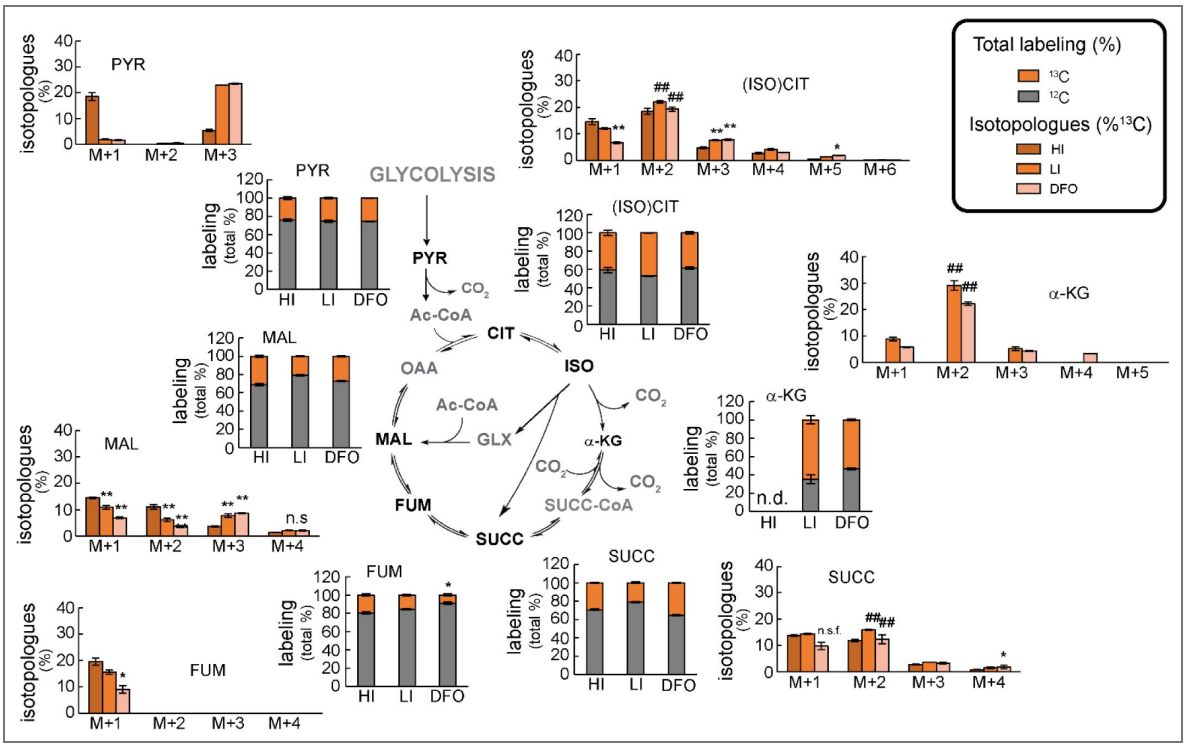

Figure 4. Percentage of labelled (^{13}C) and unlabelled (^{12}C) metabolites in the Erdman strain.

Metabolites were extracted from cells fed with $^{13}C_3$-glycerol for 8 days in 50 μM $FeCl_3$ (HI: High Iron), 0 μM $FeCl_3$ (LI: Low Iron) or 0 μM $FeCl_3$+ DFO (DFO). The analysed metabolites are shown in black in the schematic pathways. For each metabolite two plots are shown. The stacked column plots show the total percentage of labelled and unlabelled molecules per each metabolite pool; the clustered column plots show the abundance in percentage of each isotopologue. The data represent the average and the standard deviation of four biological replicates from an independent experiment, representative of four independent experiments (only two for LI condition). The p-values were calculated independently between experiments and the highest value is reported. DFO/LI vs HI: ** = p value <0.01; n.s.= non-significant; n.s.f.= non-significant fold change, the observed trend change was different between independent experiments. n.d.= non-detected. M2 vs M1: ## = p value <0.01. Ac-CoA: acetyl-CoA; CIT: citrate; FUM: fumarate; α-KG: α-ketoglutarate; ISO: isocitrate; (ISO)CIT: isocitrate and citrate; MAL: malate; OAA: oxaloacetate; PYR: pyruvate; SUCC: succinate; SUCC-CoA: succinyl-CoA.

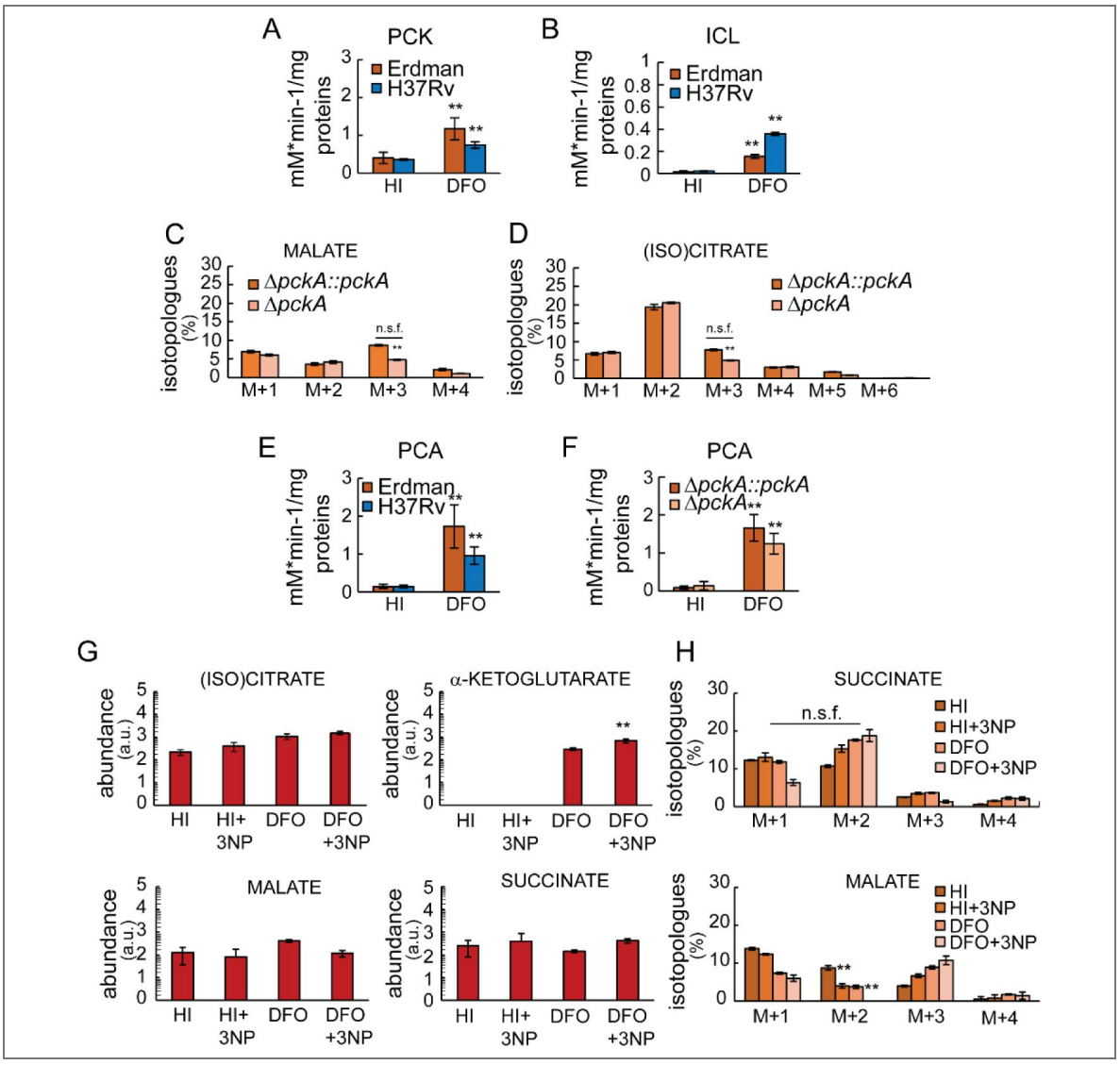

Figure 5. Analysis of iron-independent metabolic routes.

Cells were exposed to 50 μM $FeCl_3$ (HI), or 0 μM $FeCl_3$+ DFO (DFO). A) Enzymatic activity of phosphoenolpyruvate carboxykinase (PCK), reaction from phosphoenolpyruvate to oxaloacetate; B) Enzymatic activity of isocitrate lyase (ICL); the plots show the activity in (mM of NADH × min^{-1})/mg of total protein detected in cell-free extracts after 3 days of exposure to DFO or HI condition. Data show average and standard deviation from two (H37Rv) or three (Erdman strain) independent experiments and two technical replicates each (A) or from one independent experiment and three technical replicates (B). C, D) Isotopologue distribution of intracellular malate (C) and isocitrate (D) in Erdman-derived *ΔpckA::pckA* and *ΔpckA* strains after 8 days of exposure to DFO or HI conditions and fed with $^{13}C_3$-glycerol. The plots show the abundance in percentage of each isotopologue. The histograms represent average and standard deviation from four biological replicates from one experiment, representative of three independent experiments. E, F) Enzymatic activity of pyruvate carboxylase (PCA), reaction from pyruvate to oxaloacetate; the plots show the activity in (mM of NADH × min^{-1})/mg of total protein detected in cell-free extracts after 3 days of exposure to DFO or HI condition. Data show average and standard deviation from three independent experiments and two technical replicates each. G, H) Erdman strain cells were exposed to HI or DFO condition for 8 days with or without 200 μM of inhibitor 3-nitropropionate (3NP) and fed with $^{13}C_3$-glycerol. (G) The plots show the normalised levels of metabolites; the y-axis is shown on Log_{10} scale tick labels (0–5) represent the exponents of 10 (10^0–10^5); values are reported in arbitrary units. (H) The plots show the isotopologue distribution in percent abundance. The data represent the average and the standard deviation of four biological replicates from an independent experiment, representative of two independent experiments. The p-values were calculated independently between experiments and the highest value is reported. The p-values were calculated as follows. DFO vs HI for A, B, E, F; HI+3NP vs HI and DFO+3NP vs DFO for H; mutant vs complemented for C, D. n.s.f. = non-significant fold change, the observed trend change was different between independent experiments. ** = p value <0.01.

data (isotopologue distribution) on succinate, malate, and (iso)citrate (Figures 3 and 4). Oxaloacetate was not included in this analysis due to technical limitations (Supplement file Section IV). Of note, the isotopologue distribution of succinate is identical whether derived from isocitrate or from α-ketoglutarate.

Figure 3 and 4-figure supplement 1A-C show scenarios derived from pyruvate dehydrogenase (PDH) and ICL activities. M+2 (iso)citrate, malate and succinate are the only isotopologues produced. This matches the experimental results for isocitrate and succinate, for which M+2 is one of the most abundant isotopologues (Figure 3 and 4). Of note, the medium used in these experiments contains asparagine, which represents an exogenous unlabelled source of oxaloacetate (Supplement file section IV). This indicates that the Figure 3 and 4-figure supplement 1A-C scenarios are favoured and explain the dominant abundance of M+2 (iso)citrate and succinate, compared to other isotopologues. However, these combinations do not produce the most abundant malate isotopologue, M+3, detected in our measurements.

Figure 3 and 4-figure supplement 1D-S show PCK and ICL activities. In these scenarios the M+3 malate isotopologue is present and derives from the glyoxylate shunt. However, there is no congruence between these theoretical scenarios and our labelling results (more details in Supplement file section V). This raises doubts about an active role of the glyoxylate shunt in the synthesis of malate.

Figure 3 and 4-figure supplement 2A-H illustrate alternative metabolic scenarios without the involvement of the glyoxylate shunt that include PCK activity and the oxidative branch of the Krebs cycle stopping at malate. Among these scenarios, the most represented isotopologues are M+3 for (iso)citrate (Figure 3 and 4-figure supplement 2B and G), M+2 for malate and for succinate (Figure 3 and 4-figure supplement 2B, C, F and G). These scenarios offer a rationale for the observed increase in M+3 (iso)citrate in our experiments in DFO (Figure 3 and 4), and imply that M+2 malate and succinate may originate from the oxidative branch of the Krebs cycle, fed via oxaloacetate produced by PCK (Figure 3 and 4-figure supplement 2B, C, F and G). These alternative scenarios align with those showed in Figure 3 and 4-figure supplement 1A-C for the synthesis of M+2 malate and succinate, excluding the glyoxylate shunt activity, but do not reveal the origin of M+3 malate.

We then hypothesised that PEP-derived oxaloacetate could proceed to the reductive branch of Krebs cycle (Figure 3 and 4-figure supplement 2I-L). The malate isotopologues produced in the Figure 3 and 4-figure supplement 2I, K and L scenarios are all detected in our experiments. The dominance of M+3 over M+1 (Figure 3 and 4) indicates that the scenario illustrated in Figure 3 and 4-figure supplement 2I is the most likely. The minor abundance of M+4 malate (Figure 3 and 4) is compatible with the unlikely possibility that an enzyme meets both substrates labelled (Figure 3 and 4-figure supplement 2K). A similar consideration is valid for the generation of M+4/M+5/M+6 (iso)citrate and M+4 succinate (Figure 3 and 4-figure supplement 2A, E and F, Figures 3 and 4). This new analysis, which omits the glyoxylate shunt, is consistent with our experimental results and indicates that M+2 and M+4 malate derive from the oxidative branch of Krebs cycle, while M+1 and M+3 malate from the reductive branch. Further, these results indicate that, *pckA* has an important role in the CCM under Fe^{3+} starvation. Surprisingly, an Erdman-derived *pckA* mutant, which does not show loss of viability and reducing power under exposure to Fe^{3+} starvation (Figure 1F and I), does not show a significant decrease in M+3 malate and M+3 (iso)citrate in DFO (Figure 5C and D). In fact, there is no consistent between experiments (0-50% of decrease). Oxaloacetate can be produced directly from pyruvate by a pyruvate carboxylase (PCA) (Basu et al. 2018; Mukhopadhyay & Purwantini 2000), generating the same scenarios depicted in Figure 3 and 4-figure supplement 1 and 2, or malate can be directly produced from pyruvate by malic enzyme (MEZ) (Figure 3 and 4-figure supplement 2M-P). Measurement of the activity of these two enzymes in cell free extracts revealed the presence of PCA activity in the DFO condition (Figure 5E and F, Figure 5-figure supplement 1), but not of MEZ activity (Figure 5-figure supplement 1). The absence of *pckA* does not result in an increase of PCA activity (Figure 5F), suggesting that the two activities work in parallel, but serve distinct and

non-redundant functions. These results strongly suggest that *Mtb* utilises anaplerotic reactions mediated by PCK and PCA to supply Krebs cycle intermediates under Fe^{3+} starvation (Figure 3 and 4-figure supplement 2I).

The glyoxylate shunt does not supply malate and succinate under iron starvation

To provide independent, genetic evidence supporting or ruling out the role of the glyoxylate shunt under Fe^{3+} starved conditions in H37Rv, the levels of succinate, malate and isocitrate were analysed in an isocitrate lyase-deleted strain. H37Rv has two ICL enzymes, encoded by the *icl*1 and *aceAab* genes, however the second enzyme has a slower activity (Höner Zu Bentrup et al. 1999) and studies show that the inactivation of just *icl1* is relevant to alter *Mtb* physiology (Serafini et al. 2019; Gengenbacher et al. 2010). We used an H37Rv-*Δicl1* and its complemented strain (Serafini et al. 2019), which is not essential for survival in DFO condition (Figure 1E). As the *Δicl1* strain is not derived from the same H37Rv strain used in this study, metabolite abundance and isotopologue distribution in HI, LI and DFO conditions were verified and confirmed in the complemented strain (*Δicl1::icl1*). Except for the lack of increase in intra- and extracellular (iso)citrate levels, all other trends were matched (Figure 2 and 3-figure supplement 1). If the glyoxylate shunt is a key supplier of malate and succinate, the absence of a functional ICL should result in a reduction in their abundance or labelling, an increase in isocitrate levels and a decrease in the M+2 in succinate. To our surprise, there are no discernible differences between the *Δicl1* and the complemented strains, in the intracellular levels of these metabolites (Figure 2 and 3-figure supplement 2A) and in the isotopologue distribution of succinate and malate (Figure 2 and 3-figure supplement 2B and C) in DFO condition. We reasoned that in *Δicl1* metabolite secretion could be diminished to maintain the intracellular abundance of malate and succinate or increased in the case of isocitrate. Again, there are no significant differences in the extracellular levels of these metabolites between the *Δicl1* and the complemented strains (Figure 2 and 3-figure supplement 2E).

Next, we verified the operation of glyoxylate shunt in the Erdman strain by analysing the levels and labelling profiles of intracellular metabolites in DFO-treated cells exposed to a potent inhibitor of mycobacterial ICL activity, 3-nitropropionate (3NP) (Höner Zu Bentrup et al. 1999; Moynihan & Murkin 2014), which does not affect survival under such condition (Figure 2-figure supplement 3B). The presence of 3NP did not increase the abundance of (iso)citrate, but rather that of α-ketoglutarate, and no relevant changes were detected in malate and succinate levels (Figure 5G). The isotopologue distribution analysis revealed no change in the abundance of the M+2 succinate in the DFO condition, but rather a diminution of the M+2 malate (Figure 5H). 3NP is also an inhibitor of Sdh (Alston et al. 1977), and the observed result appears to report on that, instead of on inhibition of ICL. The results demonstrate that the glyoxylate shunt is not playing an important role under Fe^{3+} starvation in *Mtb*. However, the presence of isocitrate lyase activity in lysates indicates that the enzyme is active and could generate a pool of succinate, yet not detectable under our experimental conditions, likely due to compensatory metabolic routes (see below). The labelling profile analysis (Figure 3 and 4) excludes malate as a derivative of glyoxylate. We therefore investigated an alternative metabolic fate of this molecule. Glyoxylate can be converted to glycine via reductive amination catalysed by alanine dehydrogenase (Ald), whose transcript is upregulated under iron limitation (Griffin et al., 2012; Kurthkoti et al., 2017) leading us to hypothesise that this metabolic route might be active under iron starvation. Due to technical limitations, glyoxylate could not be directly detected, but we assessed glycine abundance and its isotopologue distribution (Figures 3 and 4-figure supplement 3A-D), which should mirror that of glyoxylate if glycine is derived from it. While total glycine levels were unchanged between HI and DFO conditions, isotopologue analysis revealed a ~3-fold increase in M+2 relative to M+1 under DFO in both H37Rv and Erdman strains. The comparison (Figures 3 and 4-figure supplement 3E) of these results with the most probable labelling scenarios of glyoxylate illustrated in Figures 3 and 4-figure supplements 1 and 2, suggests that glycine does not originate from glyoxylate. Additionally, no differences in labelling were observed between the *icl1* mutant and

the complemented strain (Figures 3 and 4-figure supplement 3F and G). Taken together, these results indicate that glyoxylate is not a precursor of glycine under iron starvation, further supporting the non-operational state of the glyoxylate shunt under these conditions.

The lack of evidence for an operational glyoxylate shunt under Fe^{3+} starvation led us to conclude that succinate must derive from α-ketoglutarate oxidation. The upregulation of the *korAB* genes (Kurthkoti et al. 2017) suggests that KorAB actively participates in succinyl-CoA synthesis. However, its iron-dependent nature together with the downregulation of succinyl-CoA synthetase genes (*sucCD*) suggests that an additional pathway, likely iron-independent, might be active under Fe^{3+} starvation conditions to maintain the succinate pool. This pathway might be the γ-aminobutyric acid (GABA) shunt, an active route of CCM in Mtb (Serafini et al. 2019), which converts α-ketoglutarate into succinate bypassing succinyl-CoA synthesis (Figure 5-figure supplement 2A). Genes encoding GABA shunt enzymes are not differentially expressed under Fe^{3+} starvation conditions (Dataset S1 and Kurthkoti et al. 2017; Serafini et al 2013). In H37Rv, the levels and labelling of glutamate do not change to a major extent under HI and DFO conditions (Figure 5-figure supplement 2B). In contrast, we see a significant decrease in the GABA pool size in DFO (0.001 - 0.428 FC in four independent experiments), with a concomitant decrease in total labelling (reduction >50%) (Figure 5-figure supplement 2C). Changes in GABA abundance resemble that of succinate (Figure 5-figure supplement 2D), with a greater magnitude. This suggests that GABA might be used to produce succinate. We wondered if this reduction of the GABA pool could be due to its secretion, however we were not able to detect extracellular GABA (data not shown). The isotopologue distribution of the GABA and succinate pools (Figure 5-figure supplement 2 C and D) are comparable to those of α-ketoglutarate (Figure 3) with a notable reduction in the M+1 compared to the M+2. Similar results were obtained in the Erdman strain (Figure 5-figure supplement 2E, F and G) in which the isotopologue distribution of succinate resembles that of GABA (Figure 5-figure supplement 2F and G) and glutamate, yet, it differs from that of α-ketoglutarate (Figure 4, Figure 5-figure supplement 2E). In particular, in succinate, GABA, and glutamate the levels of M+1 and M+2 are similar in DFO (Figure 5-figure supplement 2E, F and G), whereas M+2 α-ketoglutarate consistently exceeds M+1 (Figure 4). This different isotopologue distribution in α-ketoglutarate suggests that the GABA shunt is significantly sustained by other metabolic circuits beyond α-ketoglutarate in Erdman.

The absence of a differential expression of GABA shunt genes under Fe^{3+} starvation and the similarity between the labelling profiles of succinate and GABA are consistent with the hypothesis that the GABA shunt may contribute to maintaining the succinate pool under Fe^{3+} starvation conditions in *Mtb*, although direct genetic evidence is still required to substantiate this conclusion."

Discussion

This study was conducted on two *Mtb* strains that exhibit similar behavior, with minor differences likely reflecting variations in the intensity of Krebs cycle activity (SI Appendix, Section II). The results of this investigation are summarised in Figure 7. The consistent accumulation of pyruvate and α-ketoglutarate highlights two key check points controlling carbon flux through the CCM. Because DlaT and LpdC are shared components of both the pyruvate and the α-ketoglutarate dehydrogenase complexes (Tian et al. 2005; Shi & Ehrt 2006; Maksymiuk et al.2015), they likely play a critical role in this buildup. As central metabolites linking energy and carbon/nitrogen metabolism, pyruvate and α-ketoglutarate accumulation indicate that Fe^{3+} starvation slows down the overall cellular metabolism. Under these conditions, *Mtb* cells survive and maintain a physiologic energy balance (Figure 1G and H and Figure 1–supplement figure 1A and B) but display an altered redox state marked by increased NADH levels (Figure 1–supplement figure 1C and D). It has been observed that under Fe^{3+} starvation *Mtb* downregulates genes encoding the proton pumping enzymatic complexes Type I NADH dehydrogenase (*nuoABCDEFGHIJKLMN*) and cytochrome oxidase bc_1-aa_3 (*qcrCAB*/*ctaBCED*), whereas it upregulates the gene for non-proton pumping Type II NADH dehydrogenase (*ndh*) and the gene for assembly of the less efficient and non-proton pumping cytochrome oxidase *bd* (*cydABDC*) (Kurthkoti et al. 2017; Serafini et al

2013; Cruz-Ramoset al. 2004). The iron independent nature of Ndh and its lack of proton pumping activity may explain the opposite regulation of type I and II NADH dehydrogenases under Fe^{3+} starvation. In contrast, the reason behind the divergent regulation of the two cytochrome oxidases remains not clear. Together with the increased NADH/NAD ratio, these changes in the electron transport chain (ETC) suggest that the alternative ETC is less efficient at NADH reoxidation. Notably, the replacement of proton-pumping components with the non-proton pumping alternatives, along with the reported downregulation (Kurthkoti et al. 2017) of the ATP synthase operon (*atpBEFHAGDC*), contrasts with the stable ATP levels observed in Fe^{3+}-starved *Mtb* cell.

Intriguingly, the differential expression of *atpBEFHAGDC*, *ndh*, and *nuoABCDEFGHIJKLMN* genes during Fe^{3+} starvation resembles that seen during the efficient *Mtb* growth in L-lactate as a sole carbon source (Serafini et al. 2019) suggesting that *Mtb* assembles an alternative ETC tailored to distinct physiological demands. Even more intriguing is the very recent work on *M. smegmatis*, which shows that a minimal ETC composed of cytochrome oxidase *b*, Ndh and F_1F_0-ATPase can generate ATP or *pmf* using atmospheric hydrogen (Soom et al. 2025). This raises the possibility that additional, yet unidentified mechanisms support ATP synthesis under the conditions used in our study.

The downregulation of transcripts for many CCM enzymes in Fe^{3+} starvation (Kurthkoti et al. 2017; Serafini et al 2013) is presumably a consequence of the slowed carbon flux, and the induction (Kurthkoti et al. 2017; Serafini et al 2013) of a few of them (*korAB*, *pckA* and *icl1*) is likely a strategy to sustain slowed carbon flow. The induction of the iron-dependent KorAB route represents a mechanism to bypass or parallel the KDH complex and GABA shunt, in order to sustain succinate synthesis and dispose of the accumulated α-ketoglutarate. This strategy combines multiple routes to maintain succinate synthesis under Fe^{3+}-starved conditions. A combination of multiple routes is also deployed to sustain carbon flux from PEP/pyruvate to the Krebs cycle. The anaplerotic reaction of PCK converts PEP into oxaloacetate, and it is flanked by PCA, which converts pyruvate into oxaloacetate. These two activities, together with PDH, represent three routes to control the level of pyruvate and sustain the carbon flux. Detailed ^{13}C tracking through Krebs cycle intermediates revealed an unexpected split of carbon flux from PEP- and pyruvate-derived oxaloacetate to both the oxidative and reductive branches of the Krebs cycle. Oxaloacetate is partitioned between oxidation to citrate and reduction to malate, with the latter route being the most favorable (Figures 3 and 4, Figure 3 and 4-figure supplements 1 and 2). The two fluxes converge to produce malate, the extracellular level of which increases (Figure 6). The production of oxaloacetate via PCK and PCA under Fe^{3+} starvation occurs despite the presence of an exogenous source of oxaloacetate (the asparagine in the medium, Supplement file section IV), and clearly demonstrates the importance of these anaplerotic reactions under Fe^{3+} starvation beyond oxaloacetate synthesis. These activities likely control pyruvate levels but also may contribute to assimilating the excess of carbon dioxide stoichiometrically produced with α-ketoglutarate by isocitrate dehydrogenase (Icd, Figure 6). The *pckA* gene is also induced in Fe^{3+} starvation when glutamate and ammonium, but not asparagine, are present as nitrogen sources in the medium (Serafini et al. 2013) suggesting that PCK and likely PCA are the main producers of oxaloacetate under these conditions.

The significant quantities of extracellular malate under Fe^{3+} starvation, despite its intracellular levels being similar to those in Fe^{3+} replete condition, suggests that secretion of this metabolite has a functional role. Also, the reduced secretion of succinate under Fe^{3+} starvation seems to indicate that succinate (Figure 2 and Figure 2-supplement figure 1) is required to produce malate. The secretion of malate may promote carbon flux through the anaplerotic node to relieve the accumulation of metabolic intermediates from the oxidative branch of the Krebs cycle. NADH re-oxidation mediated by malate dehydrogenase, together with Ndh, may help to maintain a redox state compatible with cell survival.

The upregulation of *icl1* (Kurthkoti et al. 2017; Serafini et al. 2013) and the resulting increase of ICL activity under Fe^{3+} starvation appear to be dispensable for the synthesis of malate and succinate (Figure 2 and 3-supplement figure 2 and Figure 5), which is surprising considering

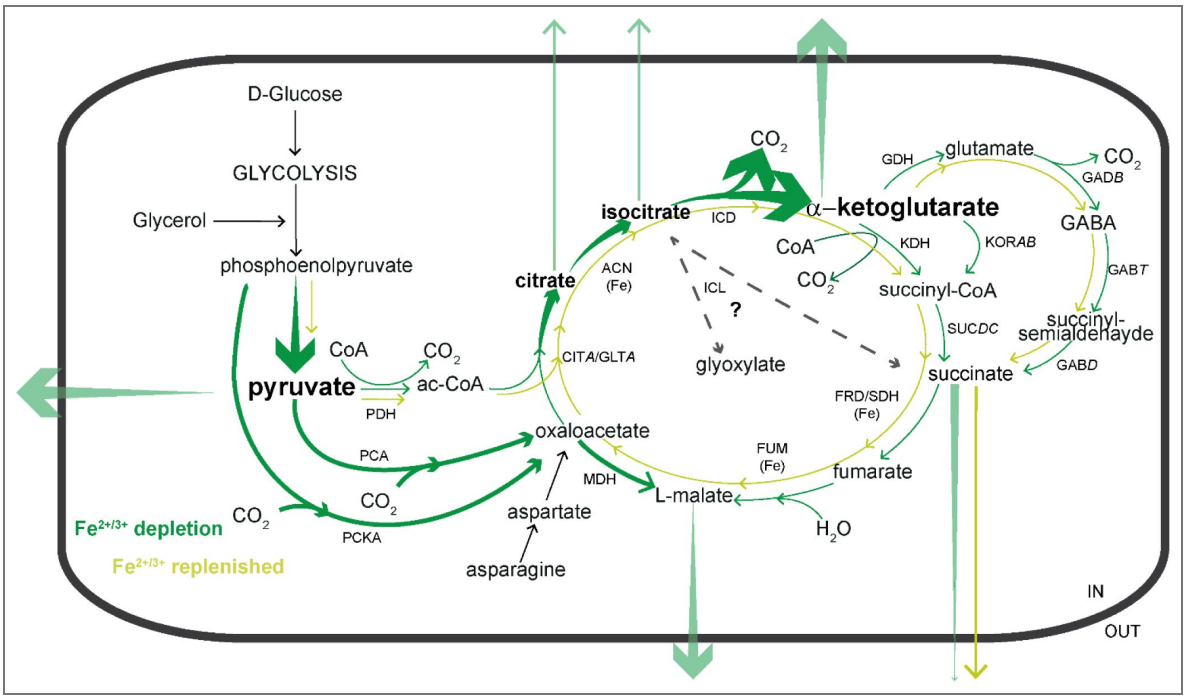

Figure 6. Re-modelling of CCM under iron starvation in *Mtb*.

The picture depicts a schematic representation of the CCM pathways active in *Mtb* exposed to Fe^{3+} deprivation in the presence of D-glucose and glycerol as carbon sources and asparagine as sole nitrogen source. The thickening arrows indicate the increase of levels of the metabolite; thicker arrows indicate a preferred route. Bold and larger font indicates accumulated metabolites. Under iron starvation, the pool of iron-dependent enzymes (denoted by Fe in parentheses in the figure) contains a reduced number of fully active molecules, which then slows the carbon flux through the Krebs cycle. The reduction in the transcript levels of iron-independent enzymes of the CCM pathways is likely a consequence of this. The disparity in efficiency between iron-dependent and iron-independent enzyme pools gives rise to the accumulation of (iso)citrate, pyruvate, and α-ketoglutarate. *Mtb* responds to these accumulations by expelling these metabolites from the cell and splitting the carbon flux from PEP/pyruvate (via PCK, PCA, and PDH activities) into both oxidative and reductive branches of the Krebs cycle. Both fluxes terminate in malate synthesis, which is then secreted. To maintain malate synthesis by succinate oxidation *Mtb* limits its secretion. Malate secretion relieves the slowdown of carbon flux through the oxidative branch of Krebs cycle. PCK and PCA anaplerotic reactions control pyruvate levels and recycle carbon dioxide stoichiometric to the α-ketoglutarate accumulation. GDH: glutamate dehydrogenase. GAD*B*: glutamate decarboxylase. GABT: 4-aminobutyrate aminotransferase. GAB*D*: succinate-semialdehyde dehydrogenase. For the other enzyme acronyms see main text.

that the glyoxylate shunt has been demonstrated to be important for the survival of *Mtb* under various growth arrest-causing conditions (Eoh & Rhee 2013; Genegenbacher et al. 2010; Nandakumar et al. 2014). On the other hand, the key function of the glyoxylate shunt is to bypass the two Krebs cycle decarboxylation reactions, and thereby "save up" carbon. Under our experimental conditions, carbon is replete, and therefore the glyoxylate shunt is not needed. Isocitrate lyase might participate in a previously unrecognised metabolic pathway or other process. The induction of ICL under Fe^{3+} starvation is not unique to mycobacteria. An increase of its activity has been observed in *Pseudomonas aeruginosa* under Fe^{3+} starvation (Ha et al. 2018) and in *Pseudomonas fluorescens* under Al^{3+} stress, which mimics iron deficiency (Middaugh et al. 2005). In *P. aeruginosa*, the absence of ICL activity causes an increase in succinate dehydrogenase activity suggesting its involvement in succinate synthesis (Ha et al. 2018). It is noteworthy that *P. aeruginosa icl* mutant accumulates intracellular iron, suggesting a role beyond CCM. Unfortunately, metabolomics studies have not been performed in this mutant. Interestingly, it has been demonstrated that *P. fluorescens* exposed to Al^{3+} stress induces an acylating glyoxylate dehydrogenase (AGODH) that transforms glyoxylate to oxalyl-CoA and then oxalate, a molecule necessary to seize Al^{3+} ions (Singh et al. 2009). Coenzyme A is recycled to produce succinyl-CoA and then succinate, releasing one ATP (Singh et al. 2009). The finding that glyoxylate is used in a metabolic pathway functional for Al^{3+} stress, rather than for malate synthesis, supports the hypothesis that *Mtb* may use ICL for an alternative metabolic function under Fe^{3+} starvation.

Collectively, these findings suggest that, under iron depletion, *Mtb* relies on anaplerotic routes to divert carbon flux from glycolysis toward the reductive branch of the Krebs cycle. This results in a truncated cycle in which both carbon fluxes converge toward malate synthesis. The secretion of malate appears to be functionally relevant to sustaining these fluxes, ensuring the production of metabolic intermediates and maintaining redox balance through NADH reoxidation via malate dehydrogenase. Although the alternative ETC comprising Ndh and cytochrome oxidase *bd*, is less efficient in both ATP synthesis and NADH reoxidation, it may represent an adaptive mechanism consistent with the reduced energetic demands of non-replicating bacteria. Under these conditions, the alternative ETC may be insufficient to fully re-oxidise NADH, thereby inducing malate dehydrogenase activity as a compensatory mechanism. This mechanistic hypothesis would explain the persistence of Mtb under iron-depleted conditions.

Further studies are needed to identify which enzymes of central carbon metabolism are essential for this mechanism. In particular, genetic and biochemical approaches targeting MDH would provide direct evidence for the role of the PCK/PCA-mediated reductive Krebs cycle in malate biosynthesis and secretion under iron-limiting conditions. Additionally, further investigation of the GABA shunt would help clarify its contribution to succinate biosynthesis.

While this study has certain limitations related to the specific experimental conditions used, these observations provide a basis for exploring whether this adaptive mechanism also occurs during infection. An important question is whether metabolites secreted by *Mtb* could substantially modify the surrounding microenvironment, thereby influencing host responses and bacterial pathogenicity.

Mycobacteria are known to exhibit a dynamic interplay between CCM and cell envelope biosynthesis under stress conditions such as hypoxia and antibiotic exposure (Eoh et al., 2022). In this context, the metabolic shift induced by iron starvation may contribute to remodelling of the cell envelope. Consistent with this, iron-starved mycobacterial cells show altered cell envelope thickness and differential expression of genes involved in mycolic acid and cell wall biosynthesis (Vijay et al., 2018; Kurthkoti, 2017). Notably, under iron starvation *Mtb* displays differential sensitivity to antibiotics with distinct structural properties: resistance is observed for smaller molecules such as kanamycin, D-cycloserine, ethionamide, ciprofloxacin, and isoniazid, whereas sensitivity to rifampicin, which has a larger and more complex structure, is maintained (Kurthkoti, 2017). This pattern suggests that cell envelope remodelling under iron starvation may selectively affect antibiotic permeability. Whether such changes also influence direct interactions with host cells, particularly at the bacteria surface-host cell interface remains an important question for future investigation.

Materials and Methods

Bacterial strains and growth conditions

In this study H37Rv and Erdman *M. tuberculosis* strains were used. *ΔpckA* and *ΔpckA*::*pckA* (Marrero et al. 2010) (Erdman genomic background) were kindly provided by Professor Sabine Ehrt (Weill Cornell Medicine). The *Δ*icl1 (Lee et al. 2013) strain was kindly provided by Professor Brian VanderVen (Cornell University). The *Δicl1*::*icl1* strain was previously generated (Serafini et al. 2019). For the metabolomic experiments in the Erdman genomic background, the strain *ΔpckA*::*pckA* was used (named Erdman strain in the text and figures and named *ΔpckA*::*pckA* in the comparison with *ΔpckA*). Bacteria were routinely cultivated at 37 °C in 7H9/7H10 medium supplemented with ADC (0.5% bovine serum albumin 0.2% glucose, 0.085% NaCl, 0.003% catalase), 0.05% Tween80 and 0.2% glycerol. Mutant and complemented strains were grown in the presence of selective antibiotics in the 7H9/7H10 pre-cultures. Antibiotics were added at the following concentrations: 20 µg/ml kanamycin (Km); 10 µg/ml gentamicin (Gm); 100 µg/ml hygromycin (Hyg).

For all the experiments bacteria were cultivated in minimal medium (MM; 0.5% w/v KH_2PO_4; 0.5 % w/v asparagine; 0.2% glycerol; 0.05% tyloxapol; 0.5% bovine serum albumin 0.2% D-glucose, 0.085% NaCl, pH 6.8) treated with Chelex100 resin (Sigma) at RT for 24 h, replacing Chelex 100 resin after 12 h. The resin was removed by filtration and the medium was supplemented with 40 mg/L $MgSO_4$;

0.1 mg/L $MnSO_4$ and $ZnSO_4$ 0.5 mg/L. For the labelling experiments, 0.2% glycerol was replaced with a mixture of 0.1% $^{13}C_3$-glycerol and 0.1% $^{13}C_3$-glycerol. The choice of glycerol as the labelled carbon source was based on the superior ability of H37Rv to metabolise this substrate compared to glucose (Serafini et al. 2019).

A source of Fe^{3+} (50 µM of $FeCl_3$) was added only in the control condition (High Iron, HI). All the tests of this study were performed in bacterial cells sub-cultured three times (4-7 days of growth) in MM supplemented with (HI) or without (0 µM of $FeCl_3$, Low Iron, LI) a Fe^{3+} source. To get growth arrest, twice sub-cultured bacterial cells grown without a source of Fe^{3+} were treated with the siderophore deferoxamine mesylate salt (DFO) at a final concentration of 50 ng/mL[15]. For each experiment parallel HI and LI cultures were also treated. For metabolomics samples, MM was prepared omitting tyloxapol, which interferes with LC-MS analysis (MM No Tyloxapol, MMNT).

All the growth experiments in liquid cultures were performed in standing in T75 (25 mL of culture)/T25 (10 mL of culture) flasks laid down on the incubator floor to optimise the oxygenation, with daily gentle manual shaking.

The input of cells was approximately 1×10^7 cells/mL for CFU/growth assay and 2×10^7 cells/mL for all the other analysis (metabolite content, ATP and NADH assays).

Cell viability was assessed by counting Colony Forming Unit (CFU) /mL or by spot density on 7H10/ADC plates. CFU/mL: bacterial culture was serially diluted 10-fold and 50 µL of each dilution was plated in duplicate. Spot's density: bacterial culture was diluted to 10^7 cells/mL (OD_{600} ~0.1) and subjected to four 1:10 serial dilutions (10^6 to 10^2 cells/mL); 5 µL of each dilution was spotted on the plate.

Protein extraction and enzymatic activity

Approximately 10-15 OD_{600} of a bacterial culture were harvested and washed three times with cold PBS 1X and then the pellet resuspended in 600 µL of extraction buffer (DPBS 1X and Complete EDTA-free protease inhibitor cocktail). The cells were disrupted by using acid-washed glass beads (2:1 = buffer volume: beads volume) and a refrigerated beat-beater (6.0 set, 35'' pulses/1' pause twice). After centrifugation at 13,000 rpm for 15 min at 4 °C, the supernatant was filtered with a PVDF filter tube before removal from the BLS3 laboratory. Within 6 hrs after extraction, enzymatic activity assays were performed using 10 µl of extract in a 96-well polystyrene microplate, with a final reaction volume of 200 µl. Protein content was determined using the Bradford reagent.

The anaplerotic activity of phosphoenolpyruvate carboxylase was determined as previously described (Machova et al. 2015) coupling the phosphoenolpyruvate carboxylation to oxaloacetate and malate synthesis by using malate dehydrogenase (pig heart, Sigma). The reaction was performed at 37 °C in a buffer containing HEPES/NaOH pH 7.2 100 mM, $KHCO_3$ 100 mM, DTT 37 mM, sodium phosphoenolpyruvate 2 mM, GDP 1 mM, $MgCl_2$ 2 mM, $MnCl_2$ 0.1 mM, malate dehydrogenase 3.5 U/ml, NADH 0.25 mM. The reaction was initiated by adding the $MgCl_2$ and $MnCl_2$. The decrease of absorbance at 340 nm was measured to monitor NADH oxidation.

Pyruvate carboxylase activity was determined as previously described (Mukhopadhyay & Purwantini 2000) coupling the phosphoenolpyruvate carboxylation to oxaloacetate and malate synthesis by using malate dehydrogenase. The reaction was performed at 37°C in a buffer containing Tris/HCl pH 8.0 50 mM, $KHCO_3$ 20 mM, $MgCl_2$ 8 mM, di-sodium ATP 8 mM, acetyl-CoA 50 µM, di-sodium NADH 0.2 mM, malate dehydrogenase 3.5 U/ml and sodium pyruvate 20 mM. The reaction was initiated by adding pyruvate. The decrease of absorbance at 340 nm was measured to monitor NADH oxidation.

Malic enzyme activity was determined as previously described (Basu et al. 2018). The reaction was performed at 30 °C in a buffer containing Tris/HCl pH 6.0 100 mM, $KHCO_3$ 200 mM, $MnCl_2$ 0.5 mM, NAD(P)H 0.6 mM, and sodium pyruvate 50 mM. The reaction was initiated by adding pyruvate. The decrease of absorbance at 340 nm was measured to monitor NAD(P)H oxidation.

Isocitrate lyase activity was determined as previously described (Munoz-Elias et al. 2006). The reaction was performed at 25 °C in a buffer containing MOPS-HCl pH 6.8 50 mM, $MgCl_2$ 5 mM, NADH 0.1 mM, 7U L-lactate dehydrogenase (Rabbit). The reaction was pre-incubated 5 minutes at 25 °C and then 1 mM of DL-*threo*-isocitrate was added. The decrease of absorbance at 340 nm was measured to monitor NADH oxidation.

Metabolite extraction and LC-MS analysis

Cells were sub-cultured twice in MM supplemented with 50 or 0 µM of $FeCl_3$, then washed once to remove tyloxapol and resuspended to a final absorbance of 0.2 in 10 mL of MMNT supplemented with 50, 0 µM of $FeCl_3$ and 0 µM of $FeCl_3$ +DFO. MMNT contained 0.2% of D-glucose, 0.1% of glycerol and 0.1% of (U)-^{13}C-labelled glycerol. Cultures were incubated standing at 37 °C. Intracellular polar metabolites were extracted after 8 days by mechanical rupture in an acetonitrile:methanol:water (2:2:1, v/v/v) solution as previously described (Serafini et al. 2019). Extracellular metabolites were extracted after 1, 3 and 8 days by diluting the culture-filtrate 1:5 using cold acetonitrile/methanol (1:1) supplemented with 0.1% formic acid; the samples were vigorously vortexed and stored at -20 °C for 2 hours; they were spun down for 10 minutes at 14,000 rpm and 4 °C, then filtered through 0.22 µm filter tubes.

2 µl of pellet extract and 10 µL of culture-filtrate extract were injected in a 1200 Liquid Chromatography system (Agilent) coupled to an Accurate Mass 6220 TOF (Agilent). Polar elution was performed as previously described using a gradient of two solvents, A (mQ water and 0.1% of formic acid) and B (acetonitrile and 0.1% of formic acid) (Serafini et al. 2019).

The data were analysed by Profinder B.08.00 software and Masshunter Qualitative Analysis B07.00. Intracellular metabolites were normalised by the residual peptide content detected using a BCA assay. Extracellular metabolites were normalised by total ion counts detected by Progenesis software. To plot the data, each normalised value was multiplied or divided for the same number, then the y axis plots report an arbitrary unit.

Due to technical limitations, the phosphorylated intermediates of glycolysis and oxaloacetate could not be analysed.

ATP and NADH/NAD assays

The ATP assay was performed using the Promega BacTiter-Glo Microbial Cell Viability assay (G8232). Three technical replicates (three aliquots of cells) were performed for each experiment using approximately 10^7 cells/well (0.1 OD_{600}). ATP levels were assessed using an ATP standard curve (µM) and values normalised to OD_{600}.The NADH/NAD ratio was determined using the

Promega NAD/NADH-Glo assay (G9071). Cells were collected, cooled on ice, and resuspended in a buffer containing PBS, NaOH and dodecyltrimethylammonium bromide according to the kit. The cells were then disrupted with a beat-beater (30" 6.5 power at 4 °C) and the extracts were filtered through 0.22 µm filter tubes. The levels of NADH and NAD were then determined according to the kit instructions using NAD and NADH calibration curves. Two technical replicates were performed for each experiment using approximately 3×10^7 cells. The experiments shown in Figure 1 and Figure 1- figure supplement 1 were performed in independent experimental sessions, using different batches of reagents and by different operators. These factors account for the differences in the y-axis scale.

Statistical analysis

Data were expressed as average and standard deviations. Statistical correlations of data were checked for significance using the paired Student T test (p value <0.05).

Extended Results

Section I. Intracellular and extracellular levels and isotopic distribution analysis of metabolites in LI vs DFO conditions

Few differences were detected between LI and DFO conditions. Unlike DFO, succinate levels do not decrease under LI in both H37Rv and Erdman (Figure 2A and Figure 2–figure supplement 1A), and (iso)citrate levels do not increase in LI in Erdman strain.

In H37Rv, total labelling analysis shows that labelled succinate levels were similar between LI and HI conditions (Figure 3), while they decreased in DFO, suggesting an alternative route for succinate production under LI. The isotopologue distribution of α-ketoglutarate and succinate in LI show differences compared to DFO in H37Rv (Figure 3). Succinate isotopologue distribution in LI (Figure 3) resemble (iso)citrate, with M+2 more abundant than M+1, whereas α-ketoglutarate as has only M+1 (Figure 3). This suggests that the glyoxylate shunt may be a dominant route only in LI. However, the lack of changes in the intracellular levels (Figure 2) and labelling (Figure 2 and 3-figure supplement 2D/ and data not shown) of (iso)citrate, malate and succinate in the *Δicl1* strain and its complemented strain supports the hypothesis that the glyoxylate shunt is not important under Fe^{3+} starvation. It is possible that in LI compared to DFO: i) α-ketoglutarate may be subject to a different metabolic circuit, and that ii) succinate originates from another route. The GABA shunt may represent this alternative route (Figure 5A and main text), which metabolites appear not to be significantly altered under Fe^{3+} starvation (Figure 5B, E and F). Like in DFO, M+1 GABA lacks in LI condition (Figure 5C). Overall, the minimal differences observed between LI and DFO conditions suggest that the main metabolic alterations observed in this study are directly attributable to Fe^{3+} starvation, rather than being secondary effects of growth cessation or unspecific DFO effect.

Section II. Comparison of total ^{13}C labelling in intra- and extracellular isocitrate, malate, fumarate and glutamate

A progressive increase in the total ^{13}C labelling of extracellular fumarate, glutamate, isocitrate and malate was observed over the course of one week under both DFO and HI conditions (from day 1 to day 8) (Figure 2-figure supplement 2A-H). This temporal rise in ^{13}C enrichment likely reflects the gradual incorporation of the labelled carbon through various metabolic pathways, resulting in an expanding pool of labelled metabolites.

When comparing the ^{13}C fractions at day 8 between intracellular and extracellular metabolites, in Erdman strain a marked reduction (approximately 50%) of labelling of these metabolites (Figure 2-figure supplement 2B, D, F and H, Figure 4, and Figure 5-figure supplement 2E) was observed under DFO conditions. In contrast, in H37Rv, the ^{13}C fraction of (iso)citrate and malate remained comparable between intra- and extracellular pools (Figure 3, Figure 2-figure

supplement 2C and E), whereas the ^{13}C fraction of extracellular glutamate decreased (approximately 50%) like in Erdman strain (Figure 2-figure supplement 2G and Figure 5-figure supplement 2B).

The reduced labelling of glutamate and fumarate is comparable with the metabolic bottleneck downstream of α-ketoglutarate, indicating a slowdown in ^{13}C flux beyond this metabolic node. The comparable ^{13}C fractions of intra- and extracellular (iso)citrate in H37Rv supports the hypothesis of the block at the α-ketoglutarate level, whereby newly synthesised isocitrate is exported out of the cell rather than being further metabolised through the Krebs cycle. A similar interpretation applies to malate in the H37Rv strain: malate produced from pyruvate and phosphoenolpyruvate (PEP) appears to be secreted into the extracellular space instead of being channelled into downstream pathways. The reduced ^{13}C labelling fraction observed in extracellular (iso)citrate and malate, compared to the intracellular pool in the Erdman strain suggests a different regulation of metabolite secretion in this strain. Alternatively, it may be linked to a higher activity of the Krebs cycle and, more broadly, CCM, which could favour the redistribution of newly assimilated carbon throughout the metabolic network. This latter observation may explain the differences in malate isotopologue distribution between H37Rv and Erdman strains.

Section III. Fumarate synthesis

The ^{13}C isotopic profile of fumarate does not align with that of succinate and malate (Figure 4H and L), despite the clear indication that the M+2 malate is derived from succinate (Figure 5H) and that the fumarate route is obligate. The fumarate pool has only the M+1 isotopologue. An explanation for these results may derive from the intracellular localization of the enzymatic complexes involved in the synthesis of malate. Given that succinate dehydrogenase is cell-membrane embedded, it seems reasonable to think that the other enzymes involved in the synthesis and oxidation of succinate are also localised close to the membrane. In this scenario, the succinate-derived fumarate might be immediately transformed to fumarate and difficult to detect. Therefore, the only presence of M+1 isotopologue reveals the activity of an alternative metabolic route whose enzymes are likely localised in a separated area of the bacterial cell. Fumarate is also the degradation product of arginosuccinate via ArgH/Rv1659 lyase (Paul et al. 2013) in the arginine succinate biosynthetic pathway. The entire *Arg* operon is upregulated under Fe^{3+} starvation (Kurthkoti et al. 2017) and our metabolic analysis showed a reduction of M+1 fumarate abundance under Fe^{3+} starvation. The reduction of labelling may represent a symptom of the general reduced cellular metabolism under Fe^{3+} depletion and the upregulation of the pathway a tentative to maintain free fumarate pool size sufficient for cell homeostasis.

Moreover, the presence of only the M+1 fumarate isotopologue, even in the presence of sufficient Fe^{3+}, suggests that the specific growth medium used affects the fumarate metabolism. Our previous work (Serafini et al. 2019) demonstrated a clear overlap between the isotopic profiles of fumarate, malate and succinate in cells grown in a media with different composition of C and N sources. The reasons for these differences related to the growth media used remain unclear.

Section IV. Oxaloacetate

Aspartate is usually used as a proxy for oxaloacetate analysis. However, in our experimental conditions, asparagine (38 mM) is present in the medium, feeding the intracellular aspartate pool. This results in a consistent amount of unlabelled Asn-derived oxaloacetate entering the Krebs cycle, and therefore aspartate cannot be used to track carbon flux. The reduced labelling percentage of aspartate (below 5%, data not shown) compared to the other Krebs cycle intermediates confirms that. The consistent amount of unlabelled Asn-derived oxaloacetate explains the prevalence of M+1 and M+2 isotopologues in (iso)citrate, α-ketoglutarate and succinate (Figure 3 and 4) which is likely due to PDH activity (Figure 3 and 4-figure supplement 1A-C).

Section V. Comparison of theoretical scenarios from Figure 3 and 4-figure supplement 1D-S with labelling results

Only the scenarios illustrated in the Figure 3 and 4-figure supplement 1D, E, P and Q lead to the production of M+3 malate. Despite producing M+3 malate, the Figure 3 and 4-figure supplement 1D scenario also produces M+5 isocitrate and M+4 succinate, which show low abundance in our measurements (Figure 3 and 4), suggesting that additional route/s contributes to the generation of M+3 malate. Importantly, this scenario employs two labelled acetyl-CoA molecules. Since the abundance of labelled pyruvate, the precursor of labelled acetyl-CoA, is well below 50% of the total pyruvate (Figure 3 and 4), this scenario is unlikely.

The Figure 3 and 4-figure supplement 1E scenario produces M+3 malate, M+2 succinate and M+3 (iso)citrate. M+2 succinate is significantly abundant in HI and DFO (Figure 3 and 4), whereas M+3 (iso)citrate increases in DFO condition (Figure 3 and 4) suggesting that this last isotopologue can derive from PCK-derived oxaloacetate. The Figure 3 and 4-figure supplement 1E scenario employs one labelled acetyl-CoA that is used by malate synthase (GlcB), similarly to Figure 3 and 4–figure supplement 1F scenario that employs one labelled acetyl-CoA but that is used by citrate synthase (GltA). The probability of the Figure 3 and 4-figure supplement 1E scenario should be equivalent to that of the Figure 3 and 4-figure supplement 1F scenario. The latter produces M+1 malate, which abundance decreases in DFO, M+5 (iso)citrate and M+4 succinate, which are the least abundant isotopologues of (iso)citrate and succinate and, their abundance slightly increases in DFO (Figure. 3 and 4). Additionally, the isotopologues produced in the Figure 3 and 4-figure supplement 1F combination in DFO are less abundant in our experimental data compared to those produced in the Figure 3 and 4-figure supplement 1E combination.

The Figure 3 and 4–figure supplement 1P scenario yields M+3 malate, M+2 succinate and M+3 (iso)citrate, however it derives from the combination of two labelled acetyl-CoA, making it as unlikely as the Figure 3 and 4–figure supplement 1D scenario.

Finally, the Figure 3 and 4-figure supplement 1Q scenario produces M+1 (iso)citrate, together with M+3 malate. This scenario includes one labelled acetyl-CoA that is used by GlcB, similarly to Figure 3 and 4-figure supplement 1R scenario that employs one labelled acetyl-CoA but that is used by citrate synthase (GltA). The probability of the Figure 3 and 4-figure supplement 1Q scenario should be equivalent to that of the Figure 3 and 4-figure supplement 1R scenario. The latter produces M+1 malate, M+2 succinate and M+3 (iso)citrate. Both Figure 3 and 4-figure supplement 1Q and Figure 3 and 4-figure supplement 1R produce specific isotopologues whose changes in abundance in the DFO condition compared to the HI condition show opposite directions (Figure 3 and 4).

In summary, while the four theoretical scenarios that include the glyoxylate cycle described above reflect qualitatively our labelling results, several quantitative discrepancies exist with the measured and predicted abundances of the isotopologues. These observations do not explain the increased abundance of M+3 malate consistently observed under Fe^{3+} starvation and raise doubts about the relevance of glyoxylate shunt under Fe^{3+} starvation.

Supplementary Figures

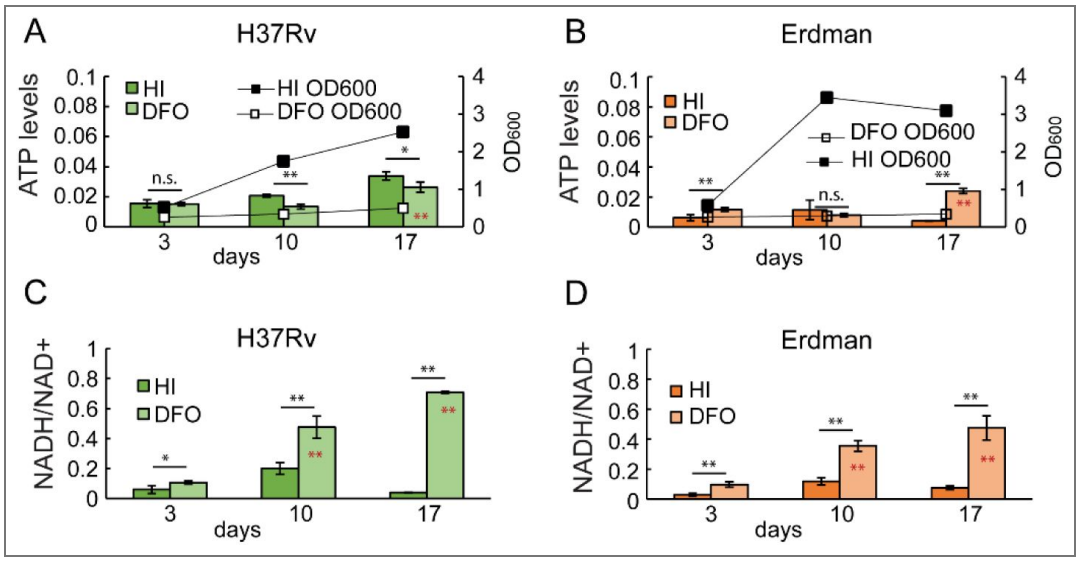

Figure 1 – figure supplement 1. Intracellular ATP content and NADH/NAD+ ratio in H37Rv and Erdman strain. Cells were exposed to 50 μM $FeCl_3$ (HI: High Iron) or 0 μM $FeCl_3$+ DFO (DFO). Samples were collected after 3, 10 and 17 days of exposure. A, B) The charts show ATP levels and growth (OD_{600}). ATP levels were calculated as μM of ATP molecules in 10^7 cells (0.1 optical density at 600 nM). C, D) The charts show the ratio between NADH and NAD levels. NADH and NAD+ levels were normalised on protein content of the extract. All the data are the average and standard deviation of two biological replicates, two culture aliquots from each replicate and two technical replicates on the 96-well plate. N.s. = non-significant, p value > 0.05. * = p value < 0.05. ** = p value < 0.01. Black asterisk (outside the bar): DFO vs HI; red asterisk (inside the bar): day 17 vs day 10 and day 3, and day 10 vs day 3.

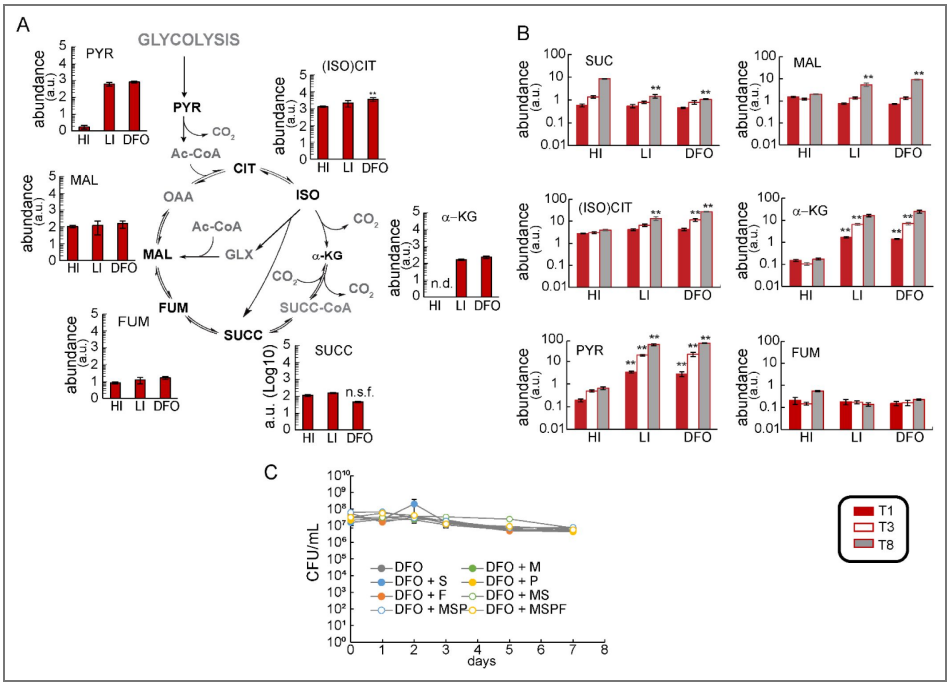

Figure 2 - figure supplement 1. Intracellular and extracellular levels of metabolites in the Erdman strain.

Cells were exposed to 50 μM $FeCl_3$ (HI: High Iron), 0 μM $FeCl_3$ (LI: Low Iron,) or 0 μM $FeCl_3$+ DFO (DFO). The analysed metabolites are shown in black in the schematic pathways. A) Intracellular polar metabolites levels at 8 days. the y-axis is shown on Log10 scale tick labels (0–5) represent the exponents of 10 (10^0–10^5); values are reported in arbitrary units. The slight decrease in succinate levels (0.66 FC) was not observed in the other four independent experiments in which no changes were observed in LI and DFO conditions compared to HI condition. B) Extracellular polar metabolites levels at 1,3 and 8 days. The plots show the normalised levels of metabolites. The y-axis is shown on is in Log_{10} scale, values are reported in arbitrary units. The data represent the average and the standard deviation of four biological replicates from an independent experiment, representative of four independent experiments for the HI and DFO conditions, and two independent experiments for the LI condition. The y axis is in Log_{10} scale, an arbitrary unit is reported. G) Viability of cells exposed to DFO in the presence of 2 mM of malate (DFO+M), succinate (DFO+S), pyruvate (DFO+P) or a combination of the three (DFO+M+S+P). The plot reports the viability measured as CFU/mL in Log_{10} scale. The data are representative of one independent experiment (average and average deviation of two technical replicates). The p-values were calculated against the HI condition and independently for the four experiments; the highest p-value is reported. * = p value < 0.05; ** = p value <0.01. n.d. = not detected. n.s.f. = not significant fold change, the observed trend change was different between independent experiments. Ac-CoA: acetyl-CoA; CIT: citrate; FUM: fumarate; α-KG: α-ketoglutarate; ISO: isocitrate; (ISO)CIT: isocitrate and citrate; MAL: malate; OAA: oxaloacetate; PYR: pyruvate SUCC: succinate; SUCC-CoA: succinyl-CoA.

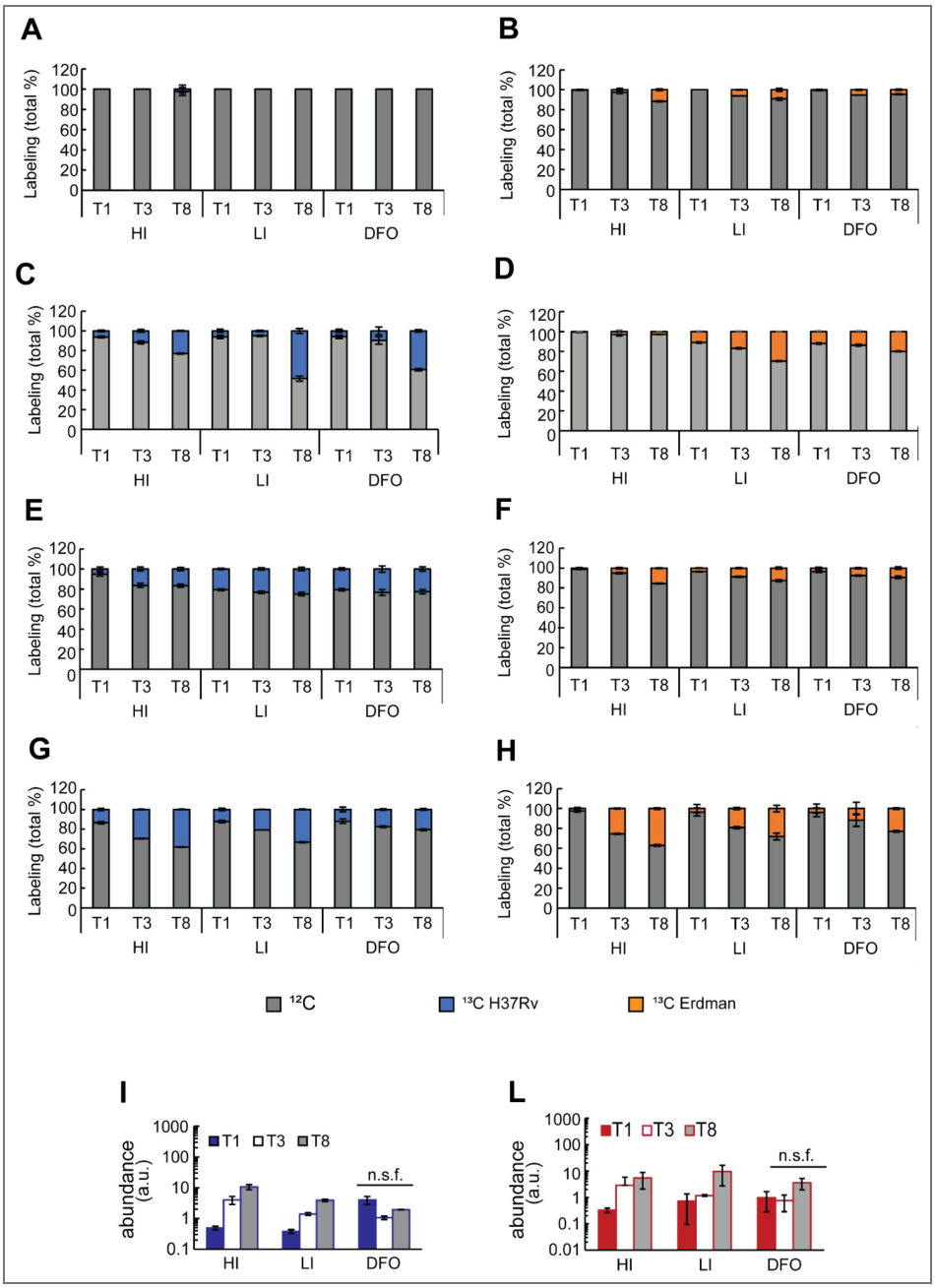

Figure 2 - figure supplement 2. Abundance and ^{13}C labelling of extracellular metabolites.

Cells were exposed to 50 µM $FeCl_3$ (HI: High Iron), 0 µM $FeCl_3$ (LI: Low Iron,) or 0 µM $FeCl_3$+ DFO (DFO). Metabolites were extracted from culture-filtrate at 1, 3 and 8 days in H37Rv (A,C,E,G,I) and Erdman strain (B,D,F,H,L). A-F) ^{13}C total labelling of fumarate (A,B), (iso)citrate (C,D) malate (E,F) and glutamate (G,H). I,L). The plots show the normalised levels of glutamate; the y axes is in log_{10} scale. The data represent the average and the standard deviation of four biological replicates from an independent experiment, representative of two independent experiments. n.s.f. = not significant fold change, the observed trend change was different between independent experiments; a.u. = arbitrary unit.

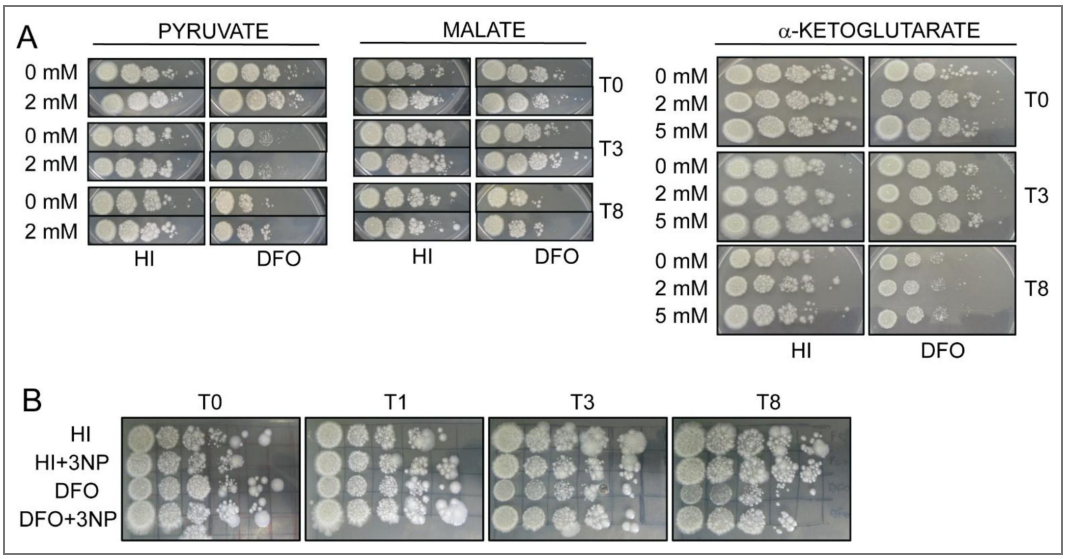

Figure 2 - figure supplement 3. Viability of *Mtb* exposed to severe Fe^{3+} starvation and in the presence of 2 mM or 5 mM Krebs cycle intermediates (A, H37Rv) or 200 µM 3NP (B, Erdman).

Cells were exposed to 50 µM $FeCl_3$ (HI: High Iron), or 0 µM $FeCl_3$+ DFO (DFO) in liquid medium for 8 days. Aliquots of cells were collected after 0, 1, 3 and 8 days, diluted to a final OD_{600} of 0.1 and 5 µL of a 10-fold serial dilution were plated on 7H10/ADC. Growth was recorded after 19-25 days.

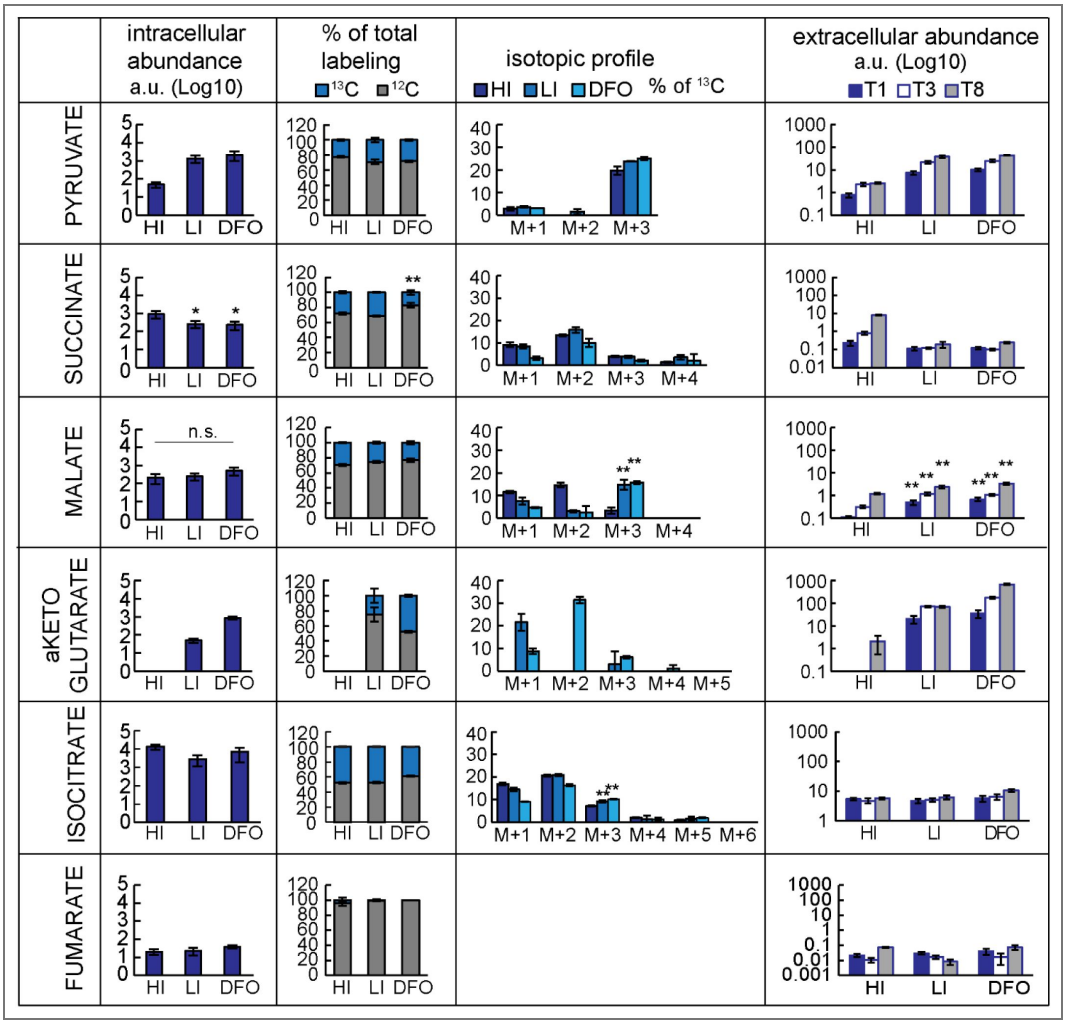

Figure 2 and 3 - figure supplement 1. Analysis of metabolites in the H37Rv-derived *Δicl1::icl1* complemented strain.

Cells were exposed to 50 μM $FeCl_3$ (HI: High Iron), 0 μM $FeCl_3$ (LI: Low Iron,) or 0 μM $FeCl_3$+ DFO (DFO), and fed with $^{13}C_3$-glycerol. Intracellular metabolites were determined after 8 days; extracellular metabolites were determined after 1,3 and 8 days. The plots show the normalised levels of metabolites. The data represent average and standard deviation from one experiment and four biological replicates. For intracellular abundance plots, the y-axis is shown on Log_{10} scale tick labels (0–5) represent the exponents of 10 (10^0–10^5), values are reported in arbitrary units. For extracellular abundance plots. The y-axis is shown on is in Log_{10} scale, values are reported in arbitrary units. The column headers contain the labels of the y axis. The p-values were calculated against HI condition. n.s. = non-significant, p value >0.05; * = p value <0.05; ** = p value <0.01. a.u. = arbitrary unit.

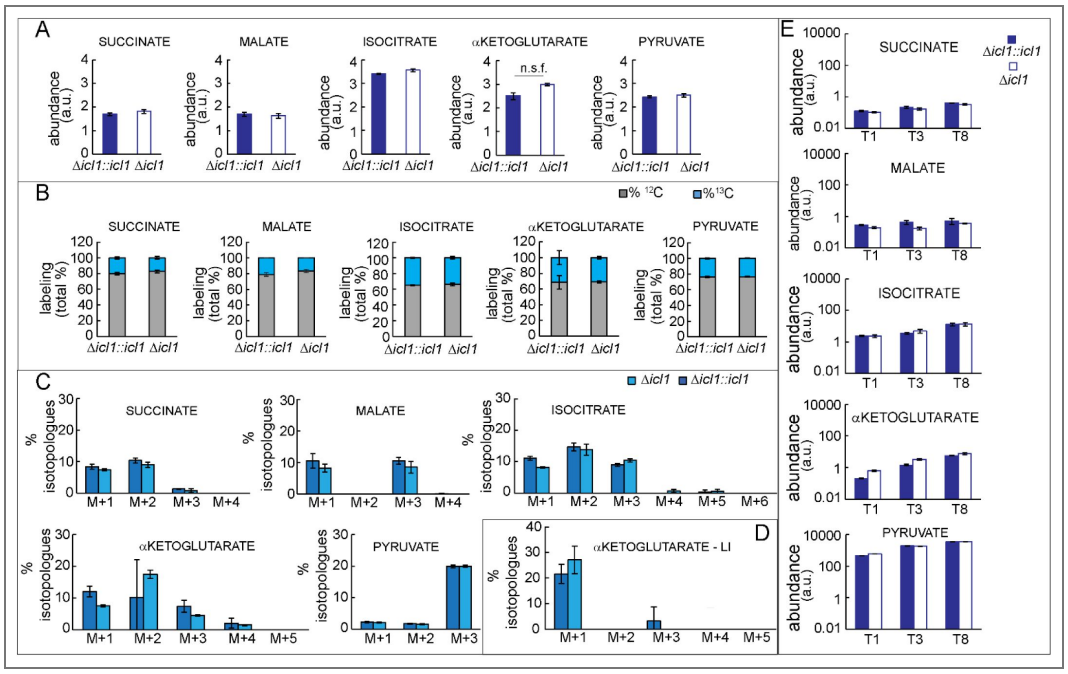

Figure 2 and 3 - figure supplement 2. Analysis of metabolites in the H37Rv-derived *icl1* mutant (*Δicl1*) compared to its complemented strain (*Δicl1::icl1*) in the DFO condition.

Cells were exposed to 0 μM $FeCl_3$+ DFO (DFO), and fed with $^{13}C_3$-glycerol for 8 days. Intracellular metabolites were extracted after 8 days; extracellular metabolites were extracted after 1,3 and 8 days. A) Normalised abundance of intracellular metabolites, the y-axis is shown on Log_{10} scale tick labels (0–4) represent the exponents of 10 (10^0–10^4), values are reported in arbitrary units. B) Total percentage of labelled and unlabelled metabolites. C) Isotopologue distribution of metabolites. D) Isotopologue distribution of the α-ketoglutarate pool in the low iron (LI; 0 μM $FeCl_3$) condition. E) Normalised abundance of extracellular metabolites, the y-axis is shown on is in Log_{10} scale, values are reported in arbitrary units. A, B, C, E) Data from one experiment representative of two independent experiments and four biological replicates. D: data from one independent experiment and four biological replicates each. The data represent average and standard deviation of four biological replicates from an independent experiment. n.s.f. = not significant fold change, the observed trend change was different between independent experiments. a.u. = arbitrary unit.

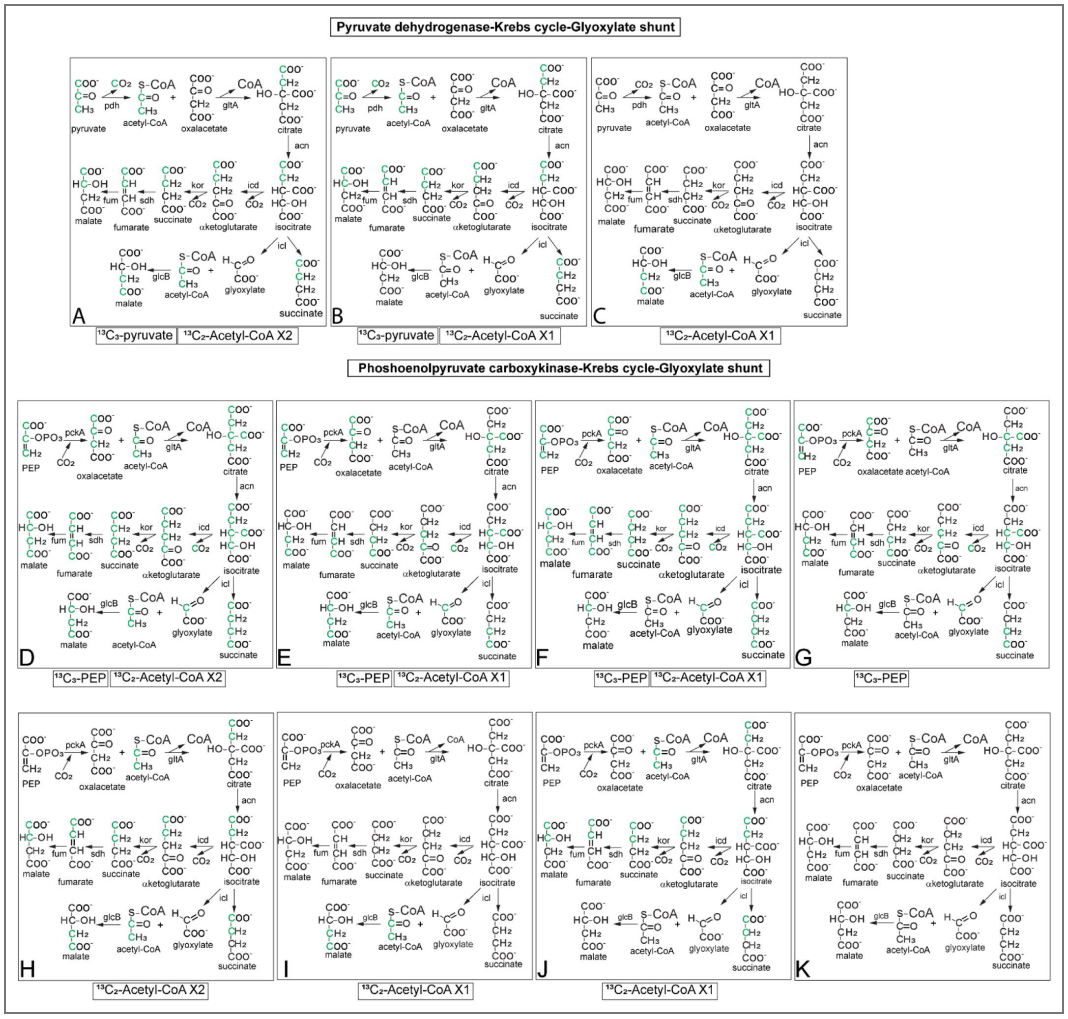

Figure 3 and 4 - figure supplement 1. Schematic representation of ^{13}C-phosphoenolpyruvate, ^{13}C-pyruvate and ^{13}C-carbon dioxide assimilation through PDH, PCK, the Krebs cycle and the glyoxylate shunt.

Atoms of ^{13}C are marked in green. The panels A-C include the activity of pyruvate dehydrogenase (PDH), the Krebs cycle and the glyoxylate shunt. The panels D-S include the activity of phosphoenolpyruvate carboxykinase (PCK), the Krebs cycle and the glyoxylate shunt. Labelled acetyl-CoA is assumed to derive from PDH activity. The bottom of each panel indicates which input metabolite is labelled. The labelling profiles of metabolites downstream to phosphoenolpyruvate (PEP) are identical if PCK is replaced by pyruvate carboxylase and PEP is replace by pyruvate. To simplify, only one of the enzymes for α-ketoglutarate degradation and citrate synthesis are reported. Acn: aconitase. GlcB: malate synthase. GltA: citrate synthase. Icd: isocitrate dehydrogenase. Icl: isocitrate lyase. Kor: αketoglutarate ferredoxin-oxidoreductase. Mdh: malate dehydrogenase. Sdh: succinate dehydrogenase.

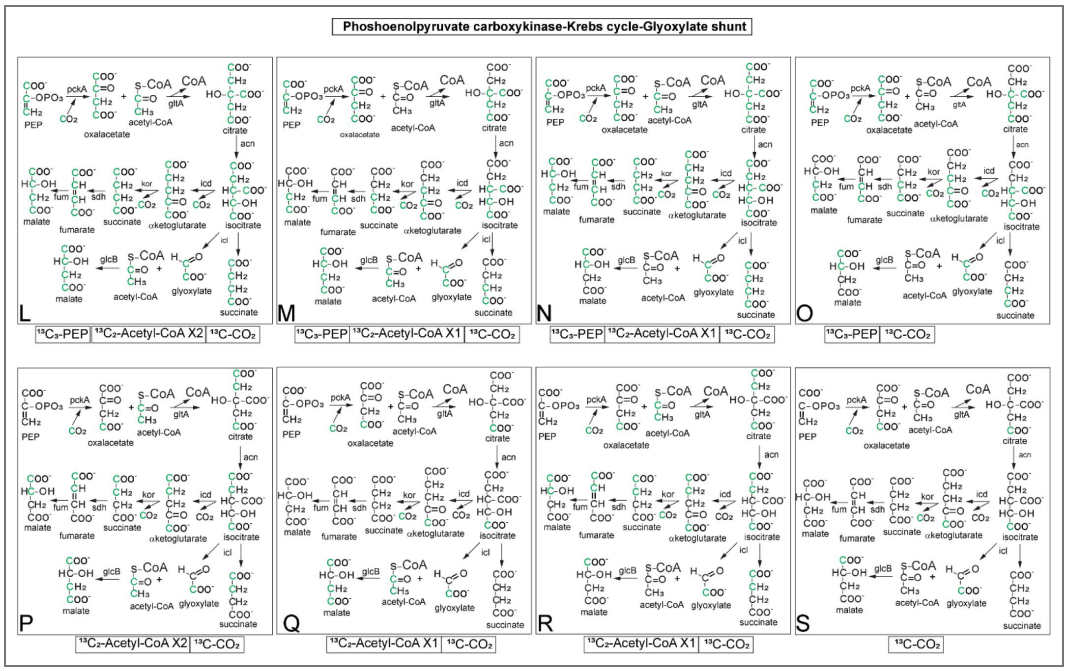

Figure 3 and 4 - figure supplement 1. (continued)

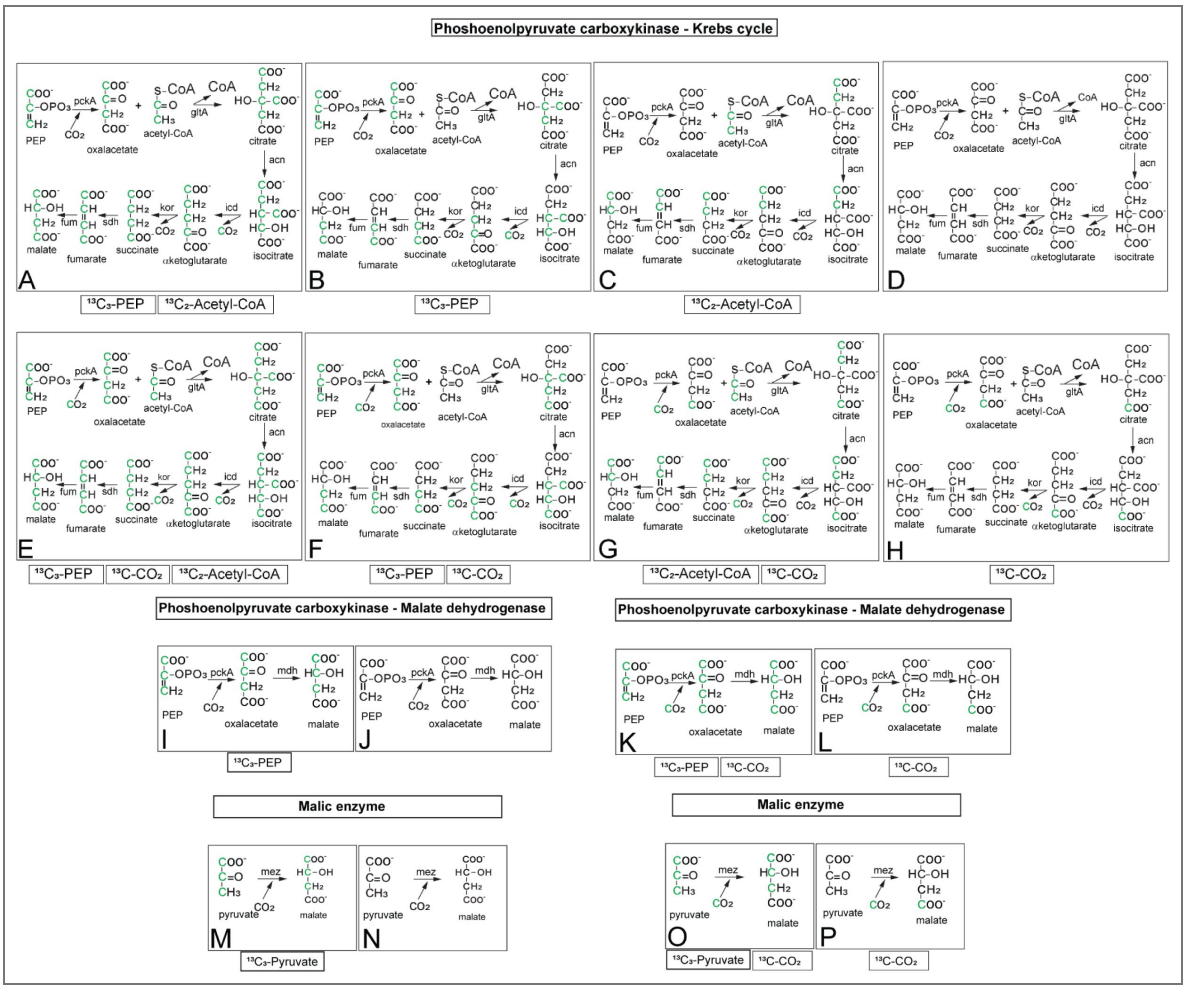

Figure 3 and 4 - figure supplement 2. Schematic representation of ^{13}C-phosphoenolpyruvate, ^{13}C-pyruvate and ^{13}C-carbon dioxide assimilation through PCK, MEZ and the Krebs cycle.

The panels A-H include the activity of phosphoenolpyruvate carboxykinase (PCK) and the Krebs cycle. Labelled acetyl-CoA is assumed to derive from PDH activity. The panels I and L include the anaplerotic reaction of PCK and the reduction of oxaloacetate to malate by MDH. The labelling profiles of metabolites downstream to phosphoenolpyruvate (PEP) are identical if PCK is replaced by pyruvate carboxylase and PEP is replaced by pyruvate (A-L). The panels M-N include the anaplerotic reaction of malic enzyme (MEZ) from pyruvate to malate. To simplify, only one of the enzymes for α-ketoglutarate degradation and citrate synthesis are reported. The bottom of each panel indicates which input metabolite is labelled. Acn: aconitase. GltA: citrate synthase. Icd: isocitrate dehydrogenase. Kor: α-ketoglutarate oxidoreductase. Sdh: succinate dehydrogenase.

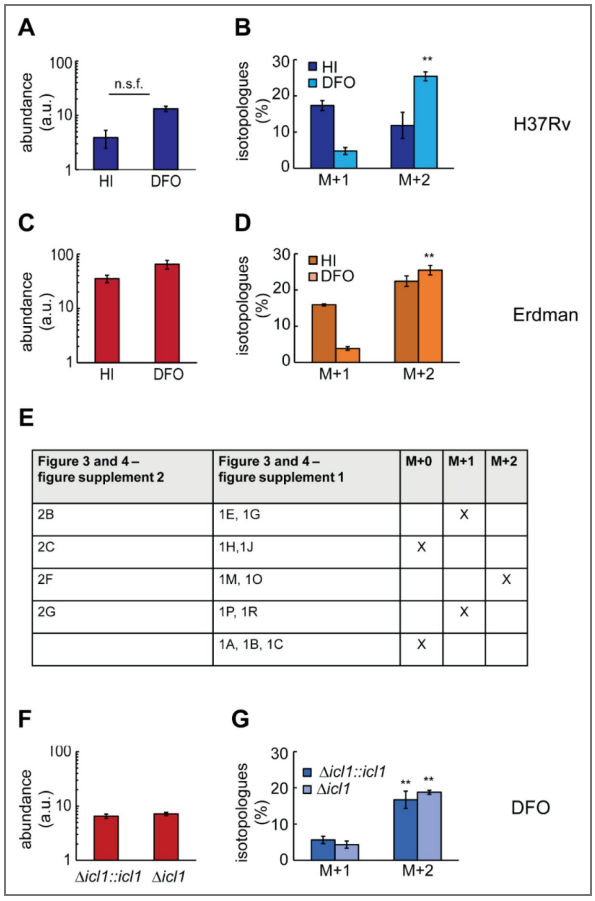

Figure 3 and 4 – figure supplement 2	Figure 3 and 4 – figure supplement 1	M+0	M+1	M+2
2B	1E, 1G		X	
2C	1H,1J	X		
2F	1M, 1O			X
2G	1P, 1R		X	
	1A, 1B, 1C	X		

Figure 3 and 4 - figure supplement 3. Analysis of intracellular glycine in the H37Rv, Erdman and H37Rv-derived icl1 mutant in HI and DFO condition.

Cells were exposed to 50 μM $FeCl_3$ (HI: High Iron), 0 μM $FeCl_3$+ DFO (DFO), and fed with $^{13}C_3$-glycerol for 8 days. A, C) Normalised levels of glycine in H37Rv and Erdman strains; the y-axis is shown on Log_{10} scale tick labels (0–5) represent the exponents of 10 (10^0–10^5), values are reported in arbitrary units. B, D) Isotopologue distribution expressed in percentage in H37Rv and Erdman strains. Plots show average and standard deviation from one experiment and four biological replicates. E) The table shows the qualitative analysis of the glycine isotopologues produced by the scenarios illustrated in the figure 3 and 4 – figure supplement 1 and 2. F) Normalised levels of glycine in an icl1 mutant and complemented strains; the y-axis is shown on is in Log_{10} scale, values are reported in arbitrary units. G) Isotopologue distribution expressed in percentage in an *icl1* mutant and complemented strains. The data are representative of two-four independent experiments. The p-values were calculated against HI condition. a.u.: arbitrary unit (see methods paragraph). n.s.f = non-significant fold change, the observed trend change was different between independent experiments. ** = p value <0.01.

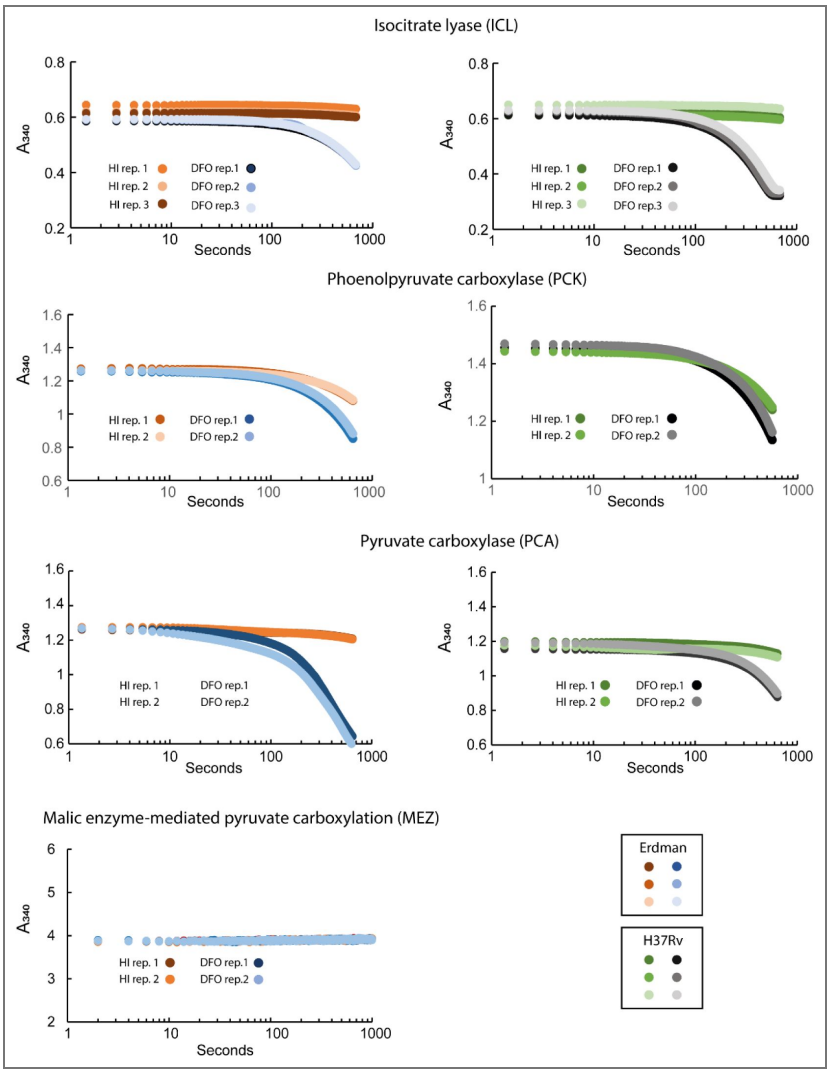

Figure 5 - figure supplement 1. ICL, PCK, PCA and MEZ activities in H37Rv and Erdman strains.

The plots report the decrease of absorbance at 340 nm due to the use of NAD(P)H or NADH from two or three technical replicates. The data are representative of one (ICL, MEZ) or two (PCK, PCA) independent experiments. The activity was performed in protein extracts from cells exposed to 50 µM $FeCl_3$ (HI: High Iron), and 0 µM $FeCl_3$+ DFO (DFO) for 3 days. The plots report the raw values not normalised on protein content.

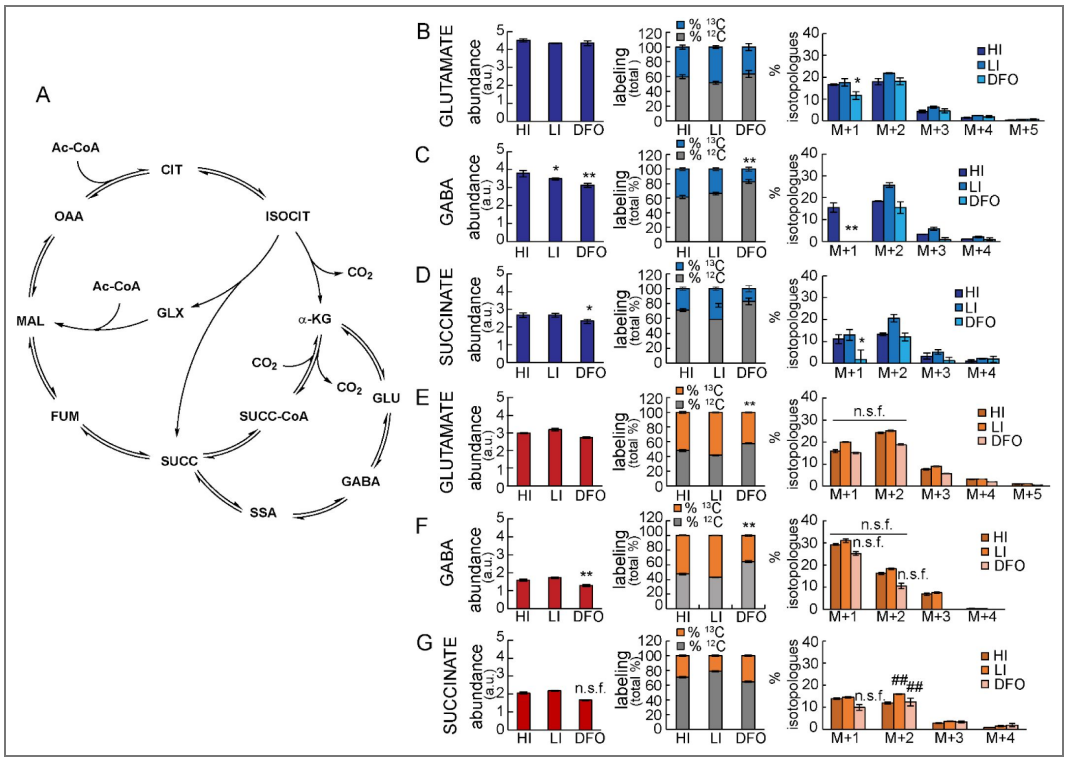

Figure 5 - figure supplement 2. Analysis of GABA shunt metabolites in H37RV and Erdman strains.

Cells were exposed to 50 μM $FeCl_3$ (HI: High Iron), 0 μM $FeCl_3$ (LI: Low Iron,) or 0 μM $FeCl_3$+ DFO (DFO), and fed with $^{13}C_3$-glycerol for 8 days. A) Schematic representation of the GABA shunt and the Krebs cycle. B, C, D) H37Rv; E, F, G) Erdman strain. B, E) glutamate; C, F) gamma-aminobutyric acid (GABA); D, G) succinate. Plots with one color-filled histograms represent the normalised levels of metabolites the y-axis is shown on Log_{10} scale tick labels (0–5) represent the exponents of 10 (10^0–10^5), values are reported in arbitrary units; plots with two color-stacked histograms represent the total abundance in percentage of labelled and unlabelled metabolite pools; plots with clustered histograms represent the abundance in percentage of each isotopologue. H37Rv data are from one experiment representative of two independent experiments and four biological replicates each; Erdman-derived strain data are from one experiment representative of four independent experiments (only two of them for the LI condition) and four biological replicates each. The histograms show average and standard deviation of four biological replicates from an independent experiment. The p-values were calculated against the HI condition; the highest p-value from the two independent experiments is shown. The differences between M+1 and M+2 isotopologues in the Erdman strain (E, F) are not significant between the three experiments, the trend varied between independent experiments. a.u.: arbitrary unit (see methods paragraph). n.s.f.= non-significant fold change, the observed trend change was different between independent experiments. DFO vs HI or LI vs HI: * =p value <0.05; ** =p value <0.01; “n.s.f.” above the individual M+1 and M+2 bars of succinate and GABA.

Data availability

Metabolomic data has been deposited in Zenodo (*10.5281/zenodo.18494375*).

Acknowledgements

Research funded by H2020 European Commission Program (MSCA-IF GA N. 101029081) and EU funding within the MUR PNRR Extended Partnership initiative on Emerging Infectious Diseases (project no. PE00000007, INF-ACT). We thank Dr Giuseppe Giordano from Pediatric Research Institute Foundation for access to the Progenesis software.

Additional information

Author's contribution

A.S. conceptualised the study, performed experiments, analysed and interpreted data, and wrote the manuscript. A.G. developed the protocol to extract metabolites from culture-filtrate samples, extracted metabolites from the culture-filtrate samples and processed the metabolomics samples in the LC-MS instrument. D.S. performed the isocitrate lyase activity experiment. L.P.S.C. critically reviewed the manuscript. A.G., D.S and R.M. contributed to revise the final draft of the manuscript.

Funding

Funder	Grant reference number	Author
EC | Horizon 2020 Framework Programme (H2020)	101029081	Riccardo Manganelli Agnese Serafini
EC | NextGenerationEU (NGEU)	PE00000007	Riccardo Manganelli

Author ORCID iDs

Agnese Serafini: https://orcid.org/0000-0002-1904-6012
Luiz Pedro Sorio de Carvalho: https://orcid.org/0000-0003-2875-4552

Additional files

Dataset 1.

References

Lopatkin AJ, Bening SC, Manson AL, Stokes JM, Kohanski MA, Badran AH, Earl AM, Cheney NJ, Yang JH, Collins JJ (2021) Clinically relevant mutations in core metabolic genes confer antibiotic resistance. *Science* **371**:eaba0862 https://doi.org/10.1126/science.aba0862 | PubMed

Hicks ND, Yang J, Zhang X, Zhao B, Grad HY, Liu L, Ou X, Chang Z, Xia H, Zhou Y, *et al.* (2018) Clinically prevalent mutations in Mycobacterium tuberculosis alter propionate metabolism and mediate multidrug tolerance. *Nat Microbiol* **3**:1032-1042 https://doi.org/10.1038/s41564-018-0218-3 | PubMed

Wang Z, Soni V, Marriner G, Kaneko T, Boshoff HIM, Barry CE, Rhee KY (2019) Mode-of-action profiling reveals glutamine synthetase as a collateral metabolic vulnerability of *M. tuberculosis* to bedaquiline. *Proc Natl Acad Sci U S A* **116**:19646-19651 https://doi.org/10.1073/pnas.1907946116 | PubMed

Kawai Y, Mercier R, Mickiewicz K, Serafini A, de Carvalho LP Sório, Errington J. (2019) Crucial role for central carbon metabolism in the bacterial L-form switch and killing by β-lactam antibiotics. *Nat Microbiol* **4**:1716-1726 https://doi.org/10.1038/s41564-019-0497-3 | PubMed

Allison KR, Brynildsen MP, Collins JJ (2011) Metabolite-enabled eradication of bacterial persisters by aminoglycosides. *Nature* **473**:216-20 https://doi.org/10.1038/nature10069 | PubMed

Lim J, Lee JJ, Lee SK, Kim S, Eum SY, Eoh H (2021) Phosphoenolpyruvate depletion mediates both growth arrest and drug tolerance of *Mycobacterium tuberculosis* in hypoxia. *Proc Natl Acad Sci U S A* **118**:e2105800118 https://doi.org/10.1073/pnas.2105800118 | PubMed

Lopatkin AJ, Stokes JM, Zheng EJ, Yang JH, Takahashi MK, You L, Collins JJ (2019) Bacterial metabolic state more accurately predicts antibiotic lethality than growth rate. *Nat Microbiol* **4**:2109-2117 https://doi.org/10.1038/s41564-019-0536-0 | PubMed

Schrader SM, Botella H, Jansen R, Ehrt S, Rhee K, Nathan C, Vaubourgeix J (2021) Multiform antimicrobial resistance from a metabolic mutation. *Sci Adv* **7**:eabh2037 https://doi.org/10.1126/sciadv.abh2037 | PubMed

WHO (2024) WHO Bacterial Priority Pathogens List 2024: Bacterial Pathogens of Public Health Importance, to Guide Research, Development, and Strategies to Prevent and Control Antimicrobial Resistance. World Health Organization, Geneva.

Murray JF, Schraufnagel DE, Hopewell PC (2015) Treatment of Tuberculosis. A Historical Perspective. *Ann Am Thorac Soc* **12**:1749-1759 https://doi.org/10.1513/AnnalsATS.201509-632PS | PubMed

Zheng X, Av-Gay Y (2016) New Era of TB Drug Discovery and Its Impact on Disease Management. *Curr Treat Options Infect Dis* **8**:299-310 https://doi.org/10.1007/s40506-016-0098-0

Dartois V, Dick T (2024) Therapeutic developments for tuberculosis and nontuberculous mycobacterial lung disease. *Nat Rev Drug Discov* **23**:381-403 https://doi.org/10.1038/s41573-024-00897-5 | PubMed

Murdoch CC, Skaar EP (2022) Nutritional immunity: the battle for nutrient metals at the host-pathogen interface. *Nat Rev Microbiol* **20**:657-670 https://doi.org/10.1038/s41579-022-00745-6 | PubMed

Serafini A (2021) Interplay between central carbon metabolism and metal homeostasis in mycobacteria and other human pathogens. *Microbiology (Reading)* **167** https://doi.org/10.1099/mic.0.001060 | PubMed

Kurthkoti K, Amin H, Marakalala MJ, Ghanny S, Subbian S, Sakatos A, Livny J, Fortune SM, Berney M, Rodriguez GM (2017) The capacity of *Mycobacterium tuberculosis* to survive iron starvation might enable it to persist in iron-deprived microenvironments of human granulomas. *mBio* **8**:e01092-17 https://doi.org/10.1128/mBio.01092-17 | PubMed

Wells RM, Jones CM, Xi Z, Speer A, Danilchanka O, Doornbos KS, Sun P, Wu F, Tian C, Nederweis M (2013) Discovery of a siderophore export system essential for virulence of Mycobacterium tuberculosis. *PLoS Pathog* **9**:e1003120 https://doi.org/10.1371/journal.ppat.1003120 | PubMed

Fang Z, Sampson SL, Warren RM, Gey van Pittius NC, Newton-Foot M. (2015) Iron acquisition strategies in mycobacteria. *Tuberculosis (Edinb)* **95**:123-30 https://doi.org/10.1016/j.tube.2015.01.004 | PubMed

Madigan CA, Martinot AJ, Wei JR, Madduri A, Cheng TY, Young DC, Layre E, Murry JP, Rubin EJ, Moody DB (2015) Lipidomic analysis links mycobactin synthase K to iron uptake and virulence in M. tuberculosis. *PLoS Pathog* **11**:e1004792 https://doi.org/10.1371/journal.ppat.1004792 | PubMed

Pisu D, Huang L, Grenier JK, Russell DG (2020) Dual RNA-Seq of Mtb-Infected Macrophages In Vivo Reveals Ontologically Distinct Host-Pathogen Interactions. *Cell Rep* **30**:335-350.e4. https://doi.org/10.1016/j.celrep.2019.12.033 | PubMed

Wong DK, Lee BY, Horwitz MA, Gibson BW (1999) Identification of fur, aconitase, and other proteins expressed by *Mycobacterium tuberculosis* under conditions of low and high concentrations of iron by combined two-dimensional gel electrophoresis and mass spectrometry. *Infect Immun* **67**:327-336 https://doi.org/10.1128/IAI.67.1.327-336.1999 | PubMed

Serafini A, Pisu D, Palù G, Rodriguez GM, Manganelli R (2013) The ESX-3 secretion system is necessary for iron and zinc homeostasis in *Mycobacterium tuberculosis*. *PLoS One* **8**:e78351 https://doi.org/10.1371/journal.pone.0078351 | PubMed

Serafini A, Tan L, Horswell S, Howell S, Greenwood DJ, Hunt DM, Phan MD, Schembri M, Monteleone M, Montague CR, *et al.* (2019) *Mycobacterium tuberculosis* requires glyoxylate shunt and reverse methylcitrate cycle for lactate and pyruvate metabolism. *Mol Microbiol* **112**:1284-1307 https://doi.org/10.1111/mmi.14362 | PubMed

Marrero J, Rhee KY, Schnappinger D, Pethe K, Ehrt S (2010) Gluconeogenic carbon flow of tricarboxylic acid cycle intermediates is critical for *Mycobacterium tuberculosis* to establish and maintain infection. *Proc Natl Acad Sci U S A* **107**:9819-9824 https://doi.org/10.1073/pnas.1000715107 | PubMed

Rao SP, Alonso S, Rand L, Dick T, Pethe K (2008) The protonmotive force is required for maintaining ATP homeostasis and viability of hypoxic, nonreplicating *Mycobacterium tuberculosis*. *Proc Natl Acad Sci U S A* **105**:11945-11950 https://doi.org/10.1073/pnas.0711697105 | PubMed

Gengenbacher M, Rao SPS, Pethe K, Dick T (2010) Nutrient-starved, non-replicating *Mycobacterium tuberculosis* requires respiration, ATP synthase and isocitrate lyase for maintenance of ATP homeostasis and viability. *Microbiology* **156**:81-87 https://doi.org/10.1099/mic.0.033084-0 | PubMed

Eoh H, Rhee KY (2013) Multifunctional essentiality of succinate metabolism in adaptation to hypoxia in *Mycobacterium tuberculosis*. *Proc Natl Acad Sci U S A* **110**:6554-6559 https://doi.org/10.1073/pnas.1219375110 | PubMed

Tian J, Bryk R, Shi S, Erdjument-Bromage H, Tempst P, Nathan C (2005) *Mycobacterium tuberculosis* appears to lack alpha-ketoglutarate dehydrogenase and encodes pyruvate dehydrogenase in widely separated genes. *Mol Microbiol* **57**:859-868 https://doi.org/10.1111/j.1365-2958.2005.04741.x | PubMed

Shi S, Ehrt S (2006) Dihydrolipoamide acyltransferase is critical for *Mycobacterium tuberculosis* pathogenesis. *Infect Immun* **74**:56-63 https://doi.org/10.1128/IAI.74.1.56-63.2006 | PubMed

Maksymiuk C, Balakrishnan A, Bryk R, Rhee KY, Nathan CF (2015) E1 of α-ketoglutarate dehydrogenase defends *Mycobacterium tuberculosis* against glutamate anaplerosis and nitroxidative stress. *Proc Natl Acad Sci U S A* **112**:E5834-5843 https://doi.org/10.1073/pnas.1510932112 | PubMed

Baughn AD, Garforth SJ, Vilchèze C, Jacobs WR (2009) An anaerobic-type alpha-ketoglutarate ferredoxin oxidoreductase completes the oxidative tricarboxylic acid cycle of *Mycobacterium tuberculosis*. *PLoS Pathog* **5**:e1000662 https://doi.org/10.1371/journal.ppat.1000662 | PubMed

Höner Zu Bentrup K, Miczak A, Swenson DL, Russell DG. (1999) Characterization of activity and expression of isocitrate lyase in *Mycobacterium avium* and *Mycobacterium tuberculosis*. *J Bacteriol* **181**:7161-7167 https://doi.org/10.1128/JB.181.23.7161-7167.1999 | PubMed

Machová I, Snašel J, Zimmermann M, Laubitz D, Plocinski P, Oehlmann W, Singh M, Dostál J, Sauer U, Pichová I (2015) *Mycobacterium tuberculosis* phosphoenolpyruvate carboxykinase is regulated by redox mechanisms and interaction with thioredoxin. *J Biol Chem* **289**:13066-13078 https://doi.org/10.1074/jbc.M113.536748 | PubMed

Basu P, Sandhu N, Bhatt A, Singh A, Balhana R, Gobe I, Crowhurst NA, Mendum TA, Gao L, Ward JL, *et al.* (2018) The anaplerotic node is essential for the intracellular survival of. *J Biol Chem* **293**:5695-5704 https://doi.org/10.1074/jbc.RA118.001839 | PubMed

Mukhopadhyay B, Purwantini E (2000) Pyruvate carboxylase from *Mycobacterium smegmatis*: stabilization, rapid purification, molecular and biochemical characterization and regulation of the cellular level. *Biochim Biophys Acta* **1475**:191-206 https://doi.org/10.1016/s0304-4165(00)00064-7 | PubMed

Moynihan MM, Murkin AS (2014) Cysteine is the general base that serves in catalysis by isocitrate lyase and in mechanism-based inhibition by 3-nitropropionate. *Biochemistry* **53**:178-187 https://doi.org/10.1021/bi401432t | PubMed

Alston TA, Mela L, Bright HJ (1977) 3-Nitropropionate, the toxic substance of Indigofera, is a suicide inactivator of succinate dehydrogenase. *Proc Natl Acad Sci U S A* **74**:3767-3771 https://doi.org/10.1073/pnas.74.9.3767 | PubMed

Giffin MM, Modesti L, Raab RW, Wayne LG, Sohaskey CD (2012) . ald of *Mycobacterium tuberculosis* encodes both the alanine dehydrogenase and the putative glycine dehydrogenase. *J Bacteriol* **194**:1045-1054 https://doi.org/10.1128/JB.05914-11 | PubMed

Cruz-Ramos H, Cook GM, Wu G, Cleeter MW, Poole RK (2004) Membrane topology and mutational analysis of *Escherichia coli* CydDC, an ABC-type cysteine exporter required for cytochrome assembly. *Microbiology (Reading)* **150**:3415-3427 https://doi.org/10.1099/mic.0.27191-0 | PubMed

Soom S, Moning SU, Cook GM, Lingford JP, Kropp A, Tran S, Grinter R, Greening C, von Ballmoos C. (2025) ATP synthesis driven by atmospheric hydrogen concentrations. *Proceedings of the National Academy of Sciences of the United States of America* **122**:e2506353122 https://doi.org/10.1073/pnas.2506353122 | PubMed

Nandakumar M, Nathan C, Rhee KY (2014) Isocitrate lyase mediates broad antibiotic tolerance in *Mycobacterium tuberculosis*. *Nat Commun* **5**:4306 https://doi.org/10.1038/ncomms5306 | PubMed

Ha S, Shin B, Park W. (2018) Lack of glyoxylate shunt dysregulates iron homeostasis in *Pseudomonas aeruginosa*. *Microbiology (Reading)* **164**:587-599 https://doi.org/10.1099/mic.0.000623 | PubMed

Middaugh J, Hamel R, Jean-Baptiste G, Beriault R, Chenier D, Appanna VD. (2005) Aluminum triggers decreased aconitase activity via Fe-S cluster disruption and the overexpression of isocitrate dehydrogenase and isocitrate lyase: a metabolic network mediating cellular survival. *J Biol Chem* **280**:3159-3165 https://doi.org/10.1074/jbc.M411979200 | PubMed

Singh R, Lemire J, Mailloux RJ, Chénier D, Hamel R, Appanna VD (2009) An ATP and oxalate generating variant tricarboxylic acid cycle counters aluminum toxicity in *Pseudomonas fluorescens*. *PLoS One* **4**:e7344 https://doi.org/10.1371/journal.pone.0007344 | PubMed

Eoh H, Liu R, Lim J, Lee JJ, Sell P (2022) Central carbon metabolism remodeling as a mechanism to develop drug tolerance and drug resistance in *Mycobacterium tuberculosis*. *Front. Cell. Infect. Microbiol* **12**:958240 https://doi.org/10.3389/fcimb.2022.958240 | PubMed

Vijay S, Hai HT, Thu DDA, Johnson E, Pielach A, Phu NH, Thwaites GE, Thuong NTT (2018) Ultrastructural analysis of cell envelope and accumulation of lipid inclusions in clinical Mycobacterium tuberculosis isolates from sputum, oxidative stress, and iron deficiency. *Front. Microbiol* **8**:2681 https://doi.org/10.3389/fmicb.2017.02681

Lee W, VanderVen BC, Fahey RJ, Russell DG (2013) Intracellular *Mycobacterium tuberculosis* exploits host-derived fatty acids to limit metabolic stress. *Journal of Biological Chemistry* **288**:6788-6800 https://doi.org/10.1074/jbc.M112.445056 | PubMed

Munoz-Elias EJ, Upton AM, Cherian J, McKinney JD (2006) Role of the methylcitrate cycle in *Mycobacterium tuberculosis* metabolism, intracellular growth, and virulence. *Molecular Microbiology* **60**:1109-1122 https://doi.org/10.1111/j.1365-2958.2006.05155.x | PubMed

Agnese Serafini, Acely Garza-Garcia, Davide Sorze, Luiz Pedro Sorio de Carvalho, Riccardo Manganellia (2026) Mycobacterium tuberculosis partitions the Krebs cycle under iron starvation. Zenodo. https://doi.org/10.5281/zenodo.18494375

Paul A, Mishra A, Surolia A, Vijayan M (2013) Cloning, expression, purification, crystallization and preliminary X-ray studies of argininosuccinate lyase (Rv1659) from *Mycobacterium tuberculosis*. *Acta Crystallogr Sect F Struct Biol Cryst Commun* **69**:1422-1424 https://doi.org/10.1107/S1744309113031138 | PubMed

Kurthkoti K, Amin H, Marakalala MJ, Ghanny S, Subbian S, Sakatos A, Livny J, Fortune SM, Berney M, Rodriguez GM (2017) The capacity of *Mycobacterium tuberculosis* to survive iron starvation might enable it to persist in iron-deprived microenvironments of human granulomas. *mBio Aug* **8**:e01092-17 https://doi.org/10.1128/mBio.01092-17 | PubMed

Serafini A, Tan L, Horswell S, Howell S, Greenwood DJ, Hunt DM, Phan MD, Schembri M, Monteleone M, Montague CR, *et al.* (2019) *Mycobacterium tuberculosis* requires glyoxylate shunt and reverse methylcitrate cycle for lactate and pyruvate metabolism. *Mol Microbiol* **112**:1284-1307 https://doi.org/10.1111/mmi.14362 | PubMed

Peer reviews

Reviewer #1 (Public review):

M. tuberculosis exhibits metabolic flexibility, enabling it to adapt to various environmental stresses, including antibiotic treatment. In this manuscript, Serafini et al. investigate the metabolic remodeling of M. tuberculosis used to survive iron-limited conditions by employing LC-MS metabolomics and 13C isotope tracing experiments. The results demonstrate that metabolic activity in the oxidative branch of the TCA cycle slows down, while the reductive branch is reverted to facilitate the biosynthesis of malate, which is subsequently secreted.

Overall, this study is experimentally well-designed, particularly the use of 13C isotope tracing to monitor TCA cycle remodeling under iron-limited conditions. The findings are valuable as they offer potential new targets for antibiotics aimed at non-replicating M. tuberculosis occurring in the hosts.

Comments on revised version:

All concerns are well addressed.

I have one minor concern: Page 3 line 16 - Fig. 1G & H: The kinetics of ATP levels between H37Rv and Erdman seem different; Erdman induces greater ATP at days 2 and 3 after DFO treatment, which was not clear in H37Rv. Fig. 1I shows NAD/NADH ratio not NADH/NAD ratio. Please change it to NADH/NAD+ to be consistent with Supplement Fig. 1 result. Include the 17-day result of NADH/NAD+ in the discussion section to explain the different viability between the two strains.

https://doi.org/10.7554/eLife.107596.2.sa2

Reviewer #2 (Public review):

Summary:

The authors investigated the effect of prolonged iron limitation (which does stop growth but does not lead to cell death) alters central metabolism in M. tuberculosis. The major tool they used is metabolomics combined with stable isotope tracing. They show that the Krebs cycle is still active, despite the fact that it is dependent on some iron-dependent enzymes. They show that carbon flux through the oxidative branch of the Krebs cycle is stalled, resulting in the accumulation of metabolites, such as malate and alpha-ketoglutarate that are partially secreted. Apparently, the carbon flux from glycolysis is partially diverted to the reductive branch of the Krebs cycle. This is not achieved by using the glyoxylate shunt but probably through the GABA shunt. This unprecedented split of the Krebs cycle and malate secretion allows a continuous flow of carbon through the core of carbon metabolism, overcoming the metabolic stalling triggered by iron starvation.

Strengths:

Novel insight in the central metabolism of a major pathogen and its adaptation to iron starvation. Carefully conducted experimentation. Paper ends with a clear and helpful model.

Weaknesses:

The authors show some surprising and important findings, but would need a little more effort to really substantiate this. Especially the role of the GABA shunt should be genetically tested, as they did for ICL and the glyoxylate shunt.

Also, the dataset 1 is not very convincing, it is only based on transcriptomics and shown with up or down, hardly a strong base for major conclusions. The very least you want is actual differences, preferable on the protein level, where it really counts....

Comments on the revised version:

In the revised version all these points were appropriately dealt with and discussed, although some of them textually and not experimentally, but for reasons that are logical.

https://doi.org/10.7554/eLife.107596.2.sa1

Author response:

The following is the authors' response to the original reviews.

> ***eLife Assessment***
>
> *This well-designed, valuable study uses isotope tracing to analyse how iron limitation alters TCA cycle metabolism in Mycobacterium tuberculosis, revealing potential antibiotic targets for non-replicating bacteria in the host. The findings provide insights into metabolic remodelling under iron-limited conditions. Whilst some of the evidence is solid, the data around the GABA shunt is incomplete, requiring genetic validation, as was done for the glyoxylate shunt. Questions remain about the underlying mechanisms and their specific role in M. tuberculosis pathogenesis.*

We thank the Editor and the reviewers for the positive evaluation of our work and for the constructive comments, which helped us improve the manuscript. We have carefully considered all the points raised and addressed them to the best of our ability. Regarding the GABA shunt, we acknowledge that genetic validation would significantly strengthen our conclusions; as this was not feasible within the revision timeframe, we have revised the relevant section by adopting more cautious language and have included genetic validation among the future perspectives. Additionally, we have expanded the discussion to address the relevance of our findings in the context of *Mtb* pathogenesis and host-pathogen interaction. A point-by-point response to each comment is provided below.

We also made minor adjustments to the main text and figures:

We removed "normalised" from the Y-axis of Figure 1 (the data are normalised and the procedure is described in the Materials and Methods).

We rearranged the order of a paragraph in the Introduction: the first paragraph "During infection pathogenic bacteria [...] extensively investigated" has been moved down, (page 2, lines 8-12). -We edited two sentences in the Introduction (page 2, lines 4-7)

Supplementary Information: we added the following sentence at page 4, lines 23-24: "The probability of the Figure 3 and 4–figure supplement 1E scenario should be equivalent to that of the Figure 3 and 4–figure supplement 1F scenario."

We made minor typing adjustments: page 3, lines 30 and 31; page 4, lines-11-12, lines 22-24; page 5, lines 23-24; page 7, line 6; page 12, lines 28 and 32.

We added details to the Materials and Methods section at page 17, lines 1 and 19-21.

> ***Public Reviews:***
>
> ***Reviewer #1 (Public review):***

> *M. tuberculosis exhibits metabolic flexibility, enabling it to adapt to various environmental stresses, including antibiotic treatment. In this manuscript, Serafini et al. investigate the metabolic remodeling of M. tuberculosis used to survive iron-limited conditions by employing LC-MS metabolomics and 13C isotope tracing experiments. The results demonstrate that metabolic activity in the oxidative branch of the TCA cycle slows down, while the reductive branch is reverted to facilitate the biosynthesis of malate, which is subsequently secreted.*
>
> *Overall, this study is experimentally well-designed, particularly the use of 13C isotope tracing to monitor TCA cycle remodeling under iron-limited conditions. The findings are valuable as they offer potential new targets for antibiotics aimed at non-replicating M. tuberculosis occurring in the hosts. However, despite these strengths, the reviewer has concerns regarding the mechanistic basis underlying the observed metabolic remodeling and its role in M. tuberculosis pathogenesis.*

We thank the reviewer for the positive evaluation of our work and for the constructive comments. Regarding the role of the observed metabolic remodelling in *Mtb* pathogenesis, we have expanded the discussion to address this aspect, contextualising our findings within the framework of *Mtb* infection and host-pathogen interaction (page 13, line 28-37; page 14, lines 1-23). Detailed responses to each specific comment are provided below.

> *Major comments*
>
> *The authors argue that iron starvation is a physiologically relevant stressor encountered by M. tuberculosis post-infection. Using Erdman and H37Rv strains under DFO conditions, Erdman loses viability, whereas H37Rv maintains it. Nonetheless, both strains exhibit similar metabolic remodeling in the TCA cycle based upon metabolomics and isotope tracing data. The authors should clarify the specific metabolic adaptations in H37Rv that enable it to sustain viability under DFO conditions.*

We thank the reviewer for this observation. Following additional experiments performed in response to subsequent comments, we re-analysed the secreted metabolite data and monitored ATP, NADH, and NAD^+ levels over 17 days in both the Erdman and H37Rv strains. The results were concordant between the two strains, supporting the hypothesis that the decrease in CFU/mL over time does not reflect a loss of viability, but rather entry into a non-culturable state or, alternatively, an increased tendency to aggregate in liquid culture. Comments have been added at page 3, lines 16-24 and page 5, lines 30-36

A mechanistic explanation of how Mtb sustains viability under iron starvation is provided at page 13, lines 2837.

> *The authors report no significant changes in NAD/NADH and ATP levels in H37Rv and Erdman exposed to DFO conditions. They observe TCA cycle remodeling, particularly the reversal of the reaction between OAA and MAL, catalysed by malate dehydrogenase, an enzyme that uses NAD+ and NADH as cofactors. The directionality of this reaction likely depends on the relative levels of NAD+ and NADH. Additionally, other dehydrogenases, such as pyruvate DH and aKG DH, also require NAD+/NADH cofactors.*

We thank the reviewer for this important observation. We agree that the directionality of the malate dehydrogenase reaction, as well as the activity of other NAD^+/NADH-dependent dehydrogenases, is likely influenced by the redox state of the cell. We therefore measured the NADH/NAD^+ ratio over 17 days in both strains under DFO conditions. We also note that the Y-axis title in Figure 1 was incorrectly reported and has been corrected accordingly. Results and interpretation of these new data are provided at:

page 3 lines 16-21

page 11 lines 16-36

page 12 lines 1-9

page 13 lines 3-5

> *In Figure 1I, NAD+ and NADH levels are monitored only at day 3 post-exposure to DFO conditions. Since Erdman loses viability after 2-3 weeks, the authors should include measurements of NAD+, NADH, and ATP levels at weekly intervals up to 3 weeks.*

We thank the reviewer for this suggestion. As recommended, we extended the monitoring of NAD^+, NADH, and ATP levels over 17 days in both strains. Results and interpretation have been discussed together and are reported in the manuscript. Please refer to the response above for the relevant page and line references.

> *Furthermore, glycine levels - which are linked to NAD+ recycling via the conversion of glyoxylate - should be measured under both HI and DFO conditions as an indirect indicator of the NAD+/NADH ratio.*

We thank the reviewer for this comment. However, we believe that glycine levels cannot be considered a reliable indirect indicator of the NAD^+/NADH ratio, as glycine is involved in multiple metabolic pathways. It can originate from serine, threonine, glyoxylate, or protein degradation, and can be incorporated into proteins, degraded to CO_2 and NH_4^+, converted to glyoxylate, or transformed into other amino acids. Due to its metabolic versatility, therefore, glycine levels lack the specificity required to reliably reflect the cellular NAD^+/NADH ratio. In addition, we could not find a single study that claim that glycine levels can be used as indicators of NAD^+/NADH ratio.

Nevertheless, this comment prompted us to examine glycine levels and isotopologue distribution under iron deprivation. Glycine levels showed no consistent trend under DFO conditions, remaining unchanged or increasing in both the Erdman and H37Rv backgrounds.

Importantly, the isotopologue distribution analysis led us to conclude that glyoxylate is not a key precursor of glycine under iron starvation. This new analysis is described at page 10 (lines 1-20), and a new supplementary figure has been added, Figure 3 and 4 – figure supplement 3.

> *In Figure 2A, it is unclear why a 100-fold accumulation of aKG does not correspond proportionally to the accumulation of (iso)citrate.*

We thank the reviewer for this observation. We agree that this point required clarification and have added a comment addressing this apparent discrepancy in the main text at page 4, lines 12–17.

> *The authors state that fumarate, aKG, (iso)citrate, malate, and pyruvate are secreted under DFO conditions. While the secretion of aKG and pyruvate makes sense, given their marked intracellular accumulation, it is puzzling why (iso)citrate, malate, and fumarate are secreted even though there are no changes in their intracellular abundance.*
>
> *To rule out the possibility that these metabolites are released due to bacterial lysis rather than active secretion, the authors should analyze the 13C-labeled fractions of these metabolites in the culture filtrate using the M. tuberculosis culture in media containing 13C glycerol.*

We thank the reviewer for this important observation.

Regarding the possibility of cell lysis, although it cannot be completely ruled out, several observations indicate that the increase in extracellular malate was not due to lysis. If

substantial cell lysis had occurred, we would expect a general increase in all extracellular metabolites. However, the extracellular fumarate and succinate levels remained unchanged in both strains under DFO (similarly to the control conditions, HI and LI). Glutamate was detected in the culture filtrate, but its abundance increased only under HI conditions, not under DFO, in either H37Rv or Erdman. The lack of increase in extracellular glutamate, fumarate and succinate, therefore suggests that, even if some cell lysis occurred, it was minimal and did not significantly affect our observations.

Regarding the 13C-fractions, we note that it is unclear how should the labelling profile would differ if extracellular metabolite derived from cell lysis. Nevertheless, as suggested by the reviewer, we compared the labelled fractions of extracellular isocitrate, malate, fumarate and glutamate. The comparison revealed variations consistent with two blocks in the carbon flow occurring at the levels of pyruvate and alpha-ketoglutarate, resulting in a slowdown in the downstream flux.

A description of these new considerations has been added at page 5 (lines 27-36) including the Figure 2 – figure supplement 2 and a new section of SI-Appendix. Therefore, we are confident that the selective appearance of some but not all metabolites in culture filtrates is consistent with secretion but not cell lysis.

> *To validate the role of the PCK-mediated reductive TCA cycle in malate biosynthesis and secretion under DFO conditions, the authors should generate a malate dehydrogenase (MDH) knockdown strain, considering that MDH is essential, and examine the 13C labeling patterns and NAD/NADH under DFO conditions.*
>
> *The authors also observe decreased GABA abundance and overall 13C labeling in DFO conditions, suggesting that the GABA shunt is the primary route for succinate biosynthesis under DFO conditions. Thus, it is strongly recommended that the authors perform a 13C glutamate tracing experiment to directly track labeling in aKG and GABA shunt metabolites, providing more definitive evidence for the involvement of the GABA shunt.*

We thank the reviewer for these valuable suggestions. We fully agree that both experiments would significantly strengthen the conclusions of our work.

Regarding the MDH knockdown strain, we acknowledge that this experiment would provide direct validation of the PCK/PCA-mediated reductive TCA cycle in malate biosynthesis. However, generating a knockdown strain in Mtb is a technically demanding and time-consuming process, requiring several months even under optimal conditions, which makes it unfeasible within the revision timeframe. We have therefore incorporated this experiment as a future perspective in the conclusions, highlighting its importance for further validating the proposed model.

Regarding the GABA shunt, we took the reviewer's comment as an opportunity to critically re-evaluate the strength of our data. As a result, we have revised the manuscript by merging the GABA shunt discussion with the glyoxylate shunt section, while adopting more cautious language in the concluding statement to reflect its hypothetical nature. The related figures have been moved to the Supplementary Materials. These aspects have been included among the future perspectives in the conclusions. Page 11, lines 10-13; page 14, lines 3-7.

> ***Reviewer #2 (Public review):***
>
> *Summary:*
>
> *The authors investigated the effect of prolonged iron limitation (which does stop growth but does not lead to cell death), altering central metabolism in M. tuberculosis. The major tool they used is metabolomics combined with stable isotope tracing. They show*

> *that the Krebs cycle is still active, despite the fact that it is dependent on some iron-dependent enzymes. They show that carbon flux through the oxidative branch of the Krebs cycle is stalled, resulting in the accumulation of metabolites, such as malate and alphaketoglutarate, that are partially secreted. Apparently, the carbon flux from glycolysis is partially diverted to the reductive branch of the Krebs cycle. This is not achieved by using the glyoxylate shunt but probably through the GABA shunt. This unprecedented split of the Krebs cycle and malate secretion allows a continuous flow of carbon through the core of carbon metabolism, overcoming the metabolic stalling triggered by iron starvation.*
>
> *Strengths:*
>
> *Novel insight into the central metabolism of a major pathogen and its adaptation to iron starvation. Carefully conducted experimentation. The paper ends with a clear and helpful model.*
>
> *Weaknesses:*
>
> *The authors show some surprising and important findings, but they would need a little more effort to really substantiate these. Especially the role of the GABA shunt should be genetically tested, as they did for ICL and the glyoxylate shunt.*

We thank the reviewer for the positive evaluation of our work. We agree that genetic validation of the GABA shunt would significantly strengthen our conclusions. However, generating the required mutant strains in Mtb is a technically demanding and time-consuming process that is unfeasible within the revision timeframe. In light of this, we have revised the manuscript by merging the GABA shunt discussion with the glyoxylate shunt section. This reorganization contextualizes the GABA shunt within a broader discussion, while adopting more cautious language in the concluding statement to reflect its hypothetical nature. Future genetic validation, including the generation of appropriate mutant strains, has been included among the future perspectives in the conclusions.

Page 11, lines 10-13; page 14, lines 3-7.

> *Also, dataset 1 is not very convincing, it is only based on transcriptomics and shown with up or down; this is not a strong base for major conclusions. As a minimum, one would want actual differences, preferably on the protein level, where it really counts.*

We thank the reviewer for this comment. We would like to clarify that Dataset S1 compiles transcriptomic and proteomic data from previously published studies, which represent the rational basis of our investigation. These data are consistently cited throughout the manuscript. The dataset was included solely as a convenience tool for the reader, to provide easy access to the relevant published information. To avoid any misunderstanding regarding its scope, we have renamed the file to 'Dataset S1 - Publicly available transcriptomic datasets referenced in this study'. Our conclusions derive from the integration of these published data with the novel biochemical and metabolomic evidence generated in this study. Further, to assist the reading, we added a clarifying description at top of “DE” column.

> ***Recommendations for the authors:***
>
> ***Reviewer #1 (Recommendations for the authors):***
>
> *(1) Clarify the definitions of "growth defect" and "growth arrest" under LI and DFO conditions, respectively.*
>
> *(2) In Figure 2A, specify the unit of the y-axis. Is it on a log scale?*

> *(3) Raw data of metabolomics and 13C isotope tracing experiments should be either deposited in public websites or provided as a separate file.*

We thank the reviewer for these comments.

Regarding the definition of 'growth defect' and 'growth arrest': we replaced 'defect' with 'slowdown' to better reflect the observed phenotype under LI conditions.

Regarding Figure 2A: we have specified the unit of the Y-axis and clarified whether the scale is logarithmic in the figure legend. We have done that for all the figures containing charts with Y/X axis in logarithmic scale. We added secondary tick marks in the charts of Figure 5G.

Regarding raw data availability: the metabolomics data have been deposited in the Zenodo database. The reference number has been added to the manuscript."

> ***Reviewer #2 (Recommendations for the authors):***
>
> *It is mentioned that measurement of the activity of these two enzymes in cell-free extracts revealed the presence of PCA activity in the DFO condition (Figure 5E), but not of MEZ activity (data not shown). Activity measurements are a great added value, but then activities should be shown, also for MEZ.*

We thank the reviewer for this suggestion. We agree that showing enzyme activity data adds value to the manuscript. As recommended, activity measurements have been included in the supplementary materials (Figure 5 – figure supplement 1).

https://doi.org/10.7554/eLife.107596.2.sa0